



# *Fermi*-LAT Observations of Gamma-Ray Emission Towards the Outer Halo of M31

# Motivation

**Roberts 1893**

**Hubble 1929**

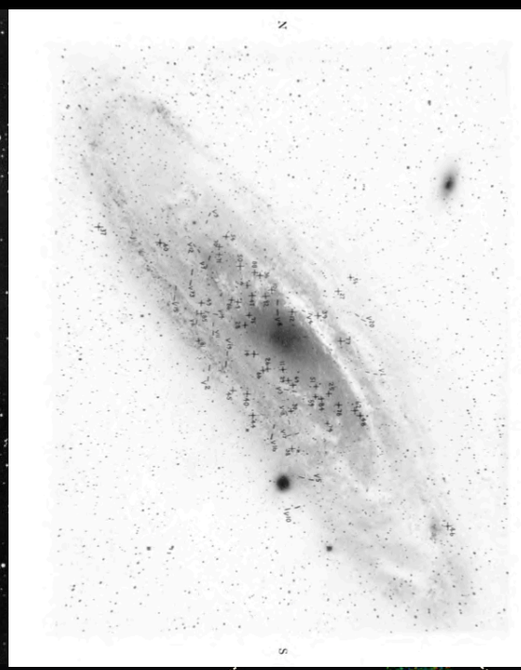


**Rubin and Ford 1970**

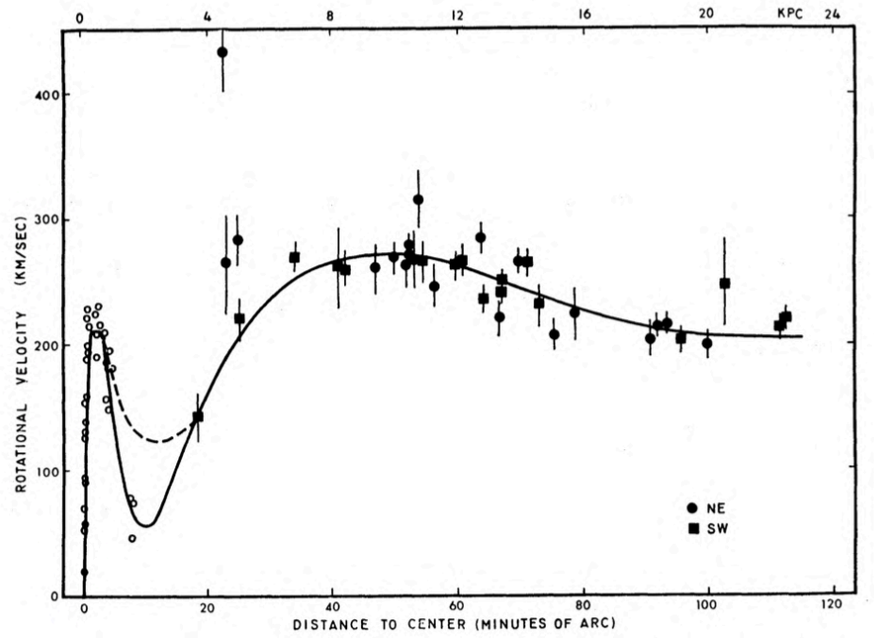


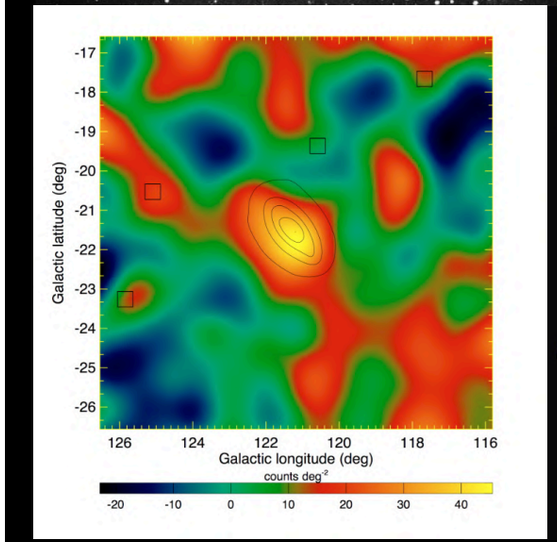


**_Fermi_-LAT 2010**

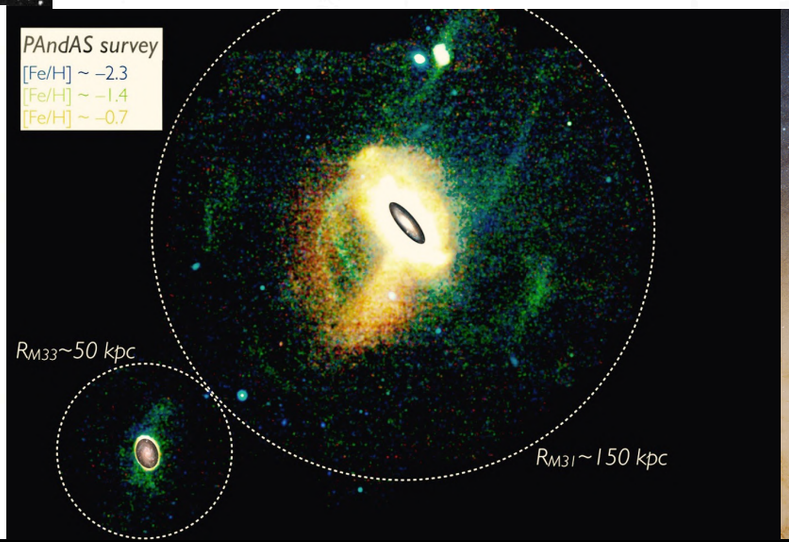


**PAndAS 2013**

**Hubble Space Telescope 2015**

- The Andromeda Galaxy is the closest spiral galaxy to us and has been the subject of numerous studies.
- LAT analysis so far has focused on the galactic disk region.
- **Our study complements previously published results on M31 and is the first to explore the farthest reaches of the M31 system in gamma-rays**.

# Motivation

## The big picture (illustrative)

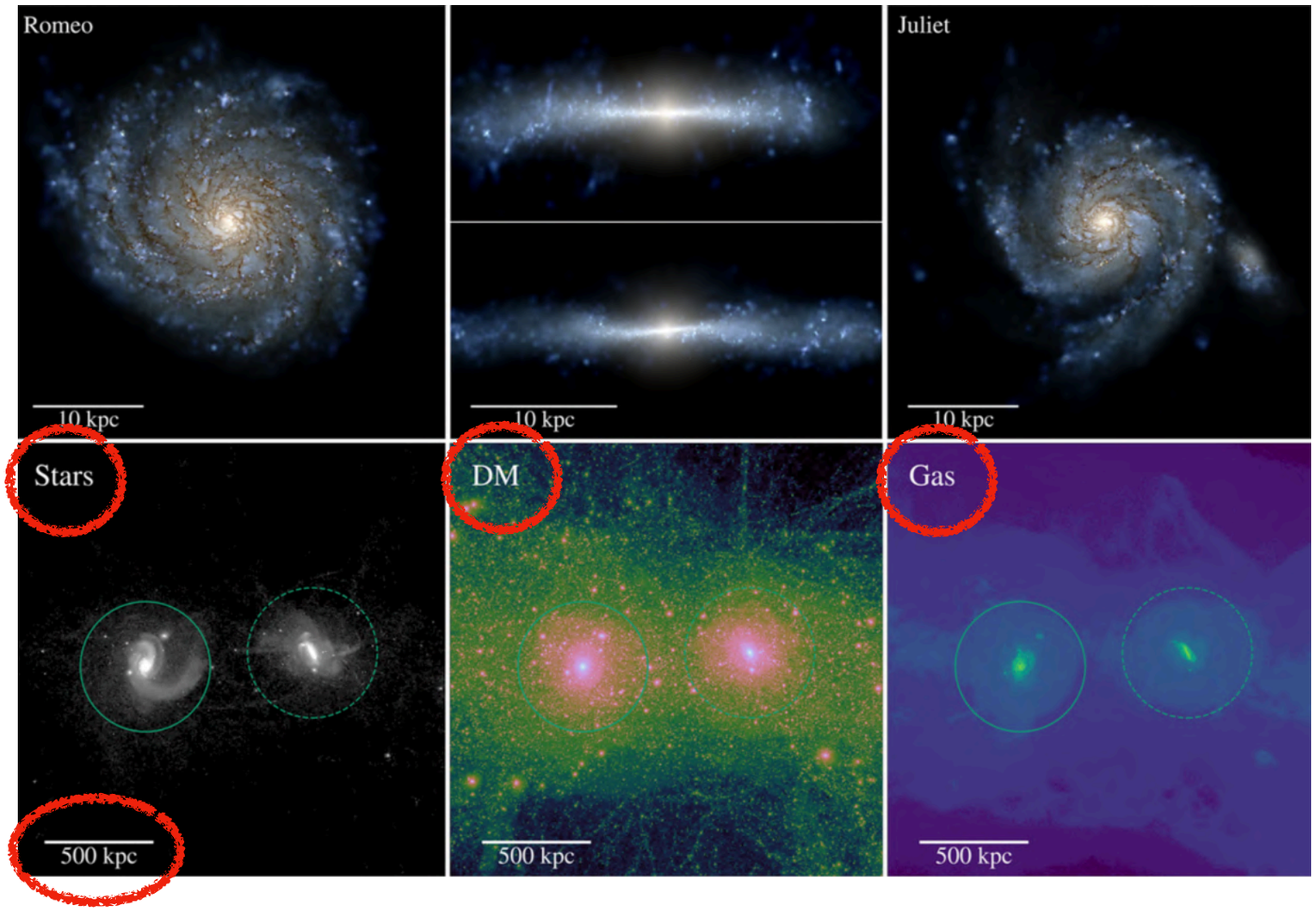


**MW-M31-Like Pairs (for example) from Garrison-Kimmel et al. 2018 (link)**

- M31 harbors a massive dark matter (DM) halo which may span up to ~600 kpc across and comprises ~90% of the galaxy's total mass.
- This halo size translates into a large diameter of 42° on the sky for an M31-Milky Way (MW) distance of 785 kpc, but its presumably low surface brightness makes it challenging to detect with gamma-ray telescopes.
- The entire M31 DM halo is seen from the outside, so we see the extended integral signal. For the MW we see through the halo, so it can be easily confused with diffuse components.
- Line of sight ostensibly includes:
  **M31 DM halo + secondary M31 emission + local DM filament between M31 and MW + MW DM halo.**

# Looking Towards the Dark Matter Halo of M31

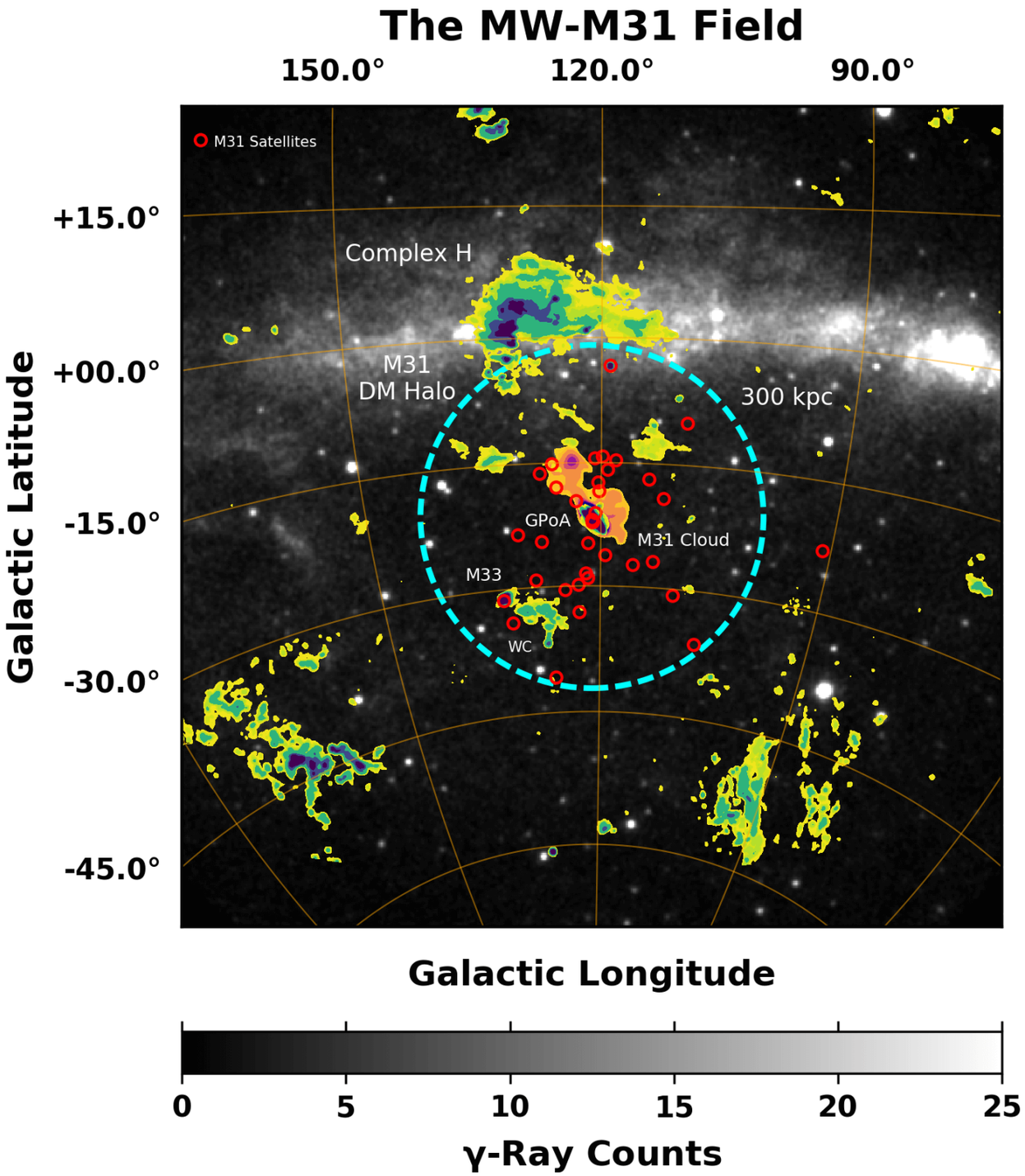


**In practice, the DM halos of M31 and the MW may deviate significantly from spherical symmetry, with an enhanced DM density in the direction of M31, relative to a gamma-ray observer inside the Milky Way.**

**As indicated by:**

- The Great Plane of Andromeda (GPoA).
- The highly lopsided distribution of M31 satellites, with ~80% lying on the side closest to the MW.
- The Vast Polar Orbital Structure of the MW.
- The local filament structure.
- The M31 cloud, with an H I mass of ~10^8-10^9 M_sun at the distance of M31.
- Complex H, with an H I mass of ~10^7 at 30 kpc from the GC.
- Simulations of MW-M31-like galaxy pairs.

# Observations

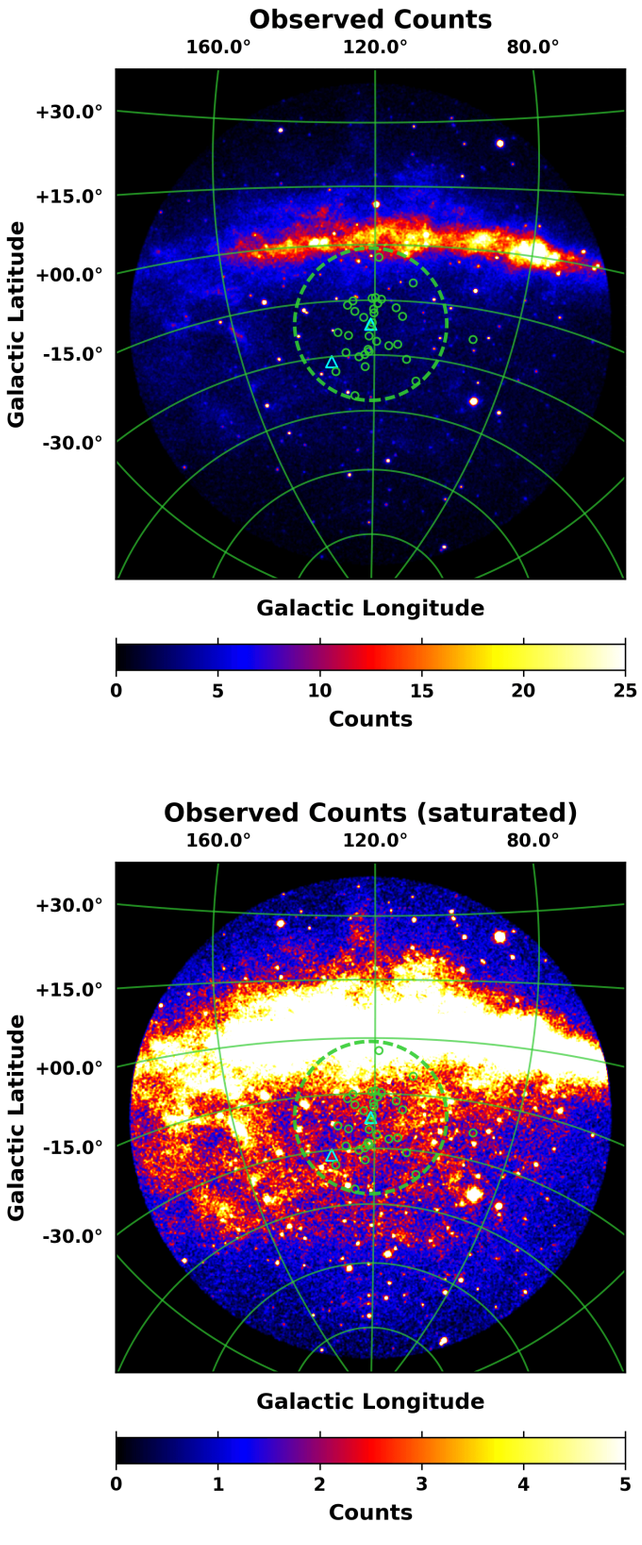


**Event Selection:**

- Front and back events, P8R2_Clean_V6 selection
- Data: 7.6 years (2008-08-04 to 2016-03-16)
- Full ROI is a 60° radius centered at the position of M31 (l,b) = (121.17°,-21.57°). Our primary field of interest, FM31, is a 28° x 28° region centered at M31.
- Energy range: 1-100 GeV in 20 bins logarithmically spaced
- Pixelation: 0.2° x 0.2°
- Fermi-LAT Science Tools v10-00-05 (run on UCI HPC, v10r0p5)

**Images:**

- Top: full count range. Bottom: saturated counts, emphasizing lower counts at high latitudes.
- Dashed green circle (21° in radius) corresponds to a 300 kpc projected radius, for an M31-MW distance of 785 kpc, i.e. the virial radius.
- M31 and M33 are shown with cyan triangles, and the rest of M31's dwarf galaxy population are shown with small green circles.
- **The primary purpose of the overlay is to provide a qualitative representation of M31's outer halo and to show its relationship to the MW disk**.
- Note: we do not expect to detect most of the M31 dwarfs, as the MW dwarfs are mostly undetected.

# GALPROP Parameters

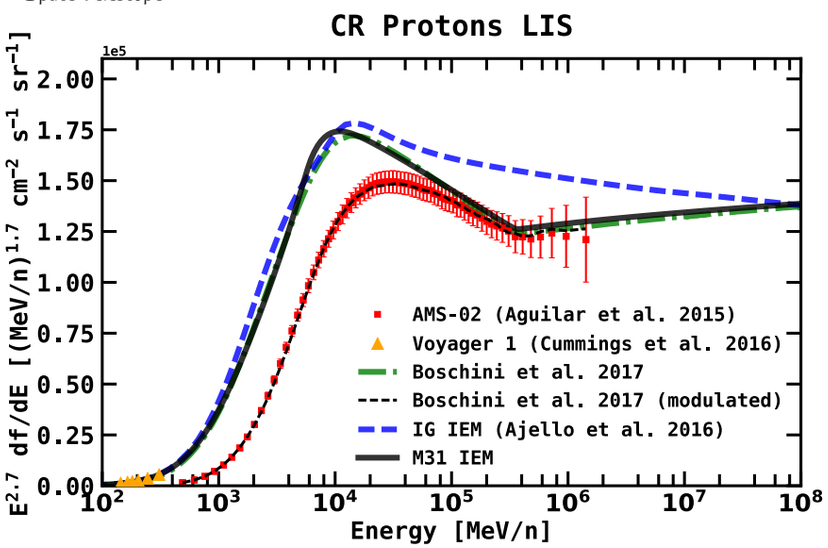


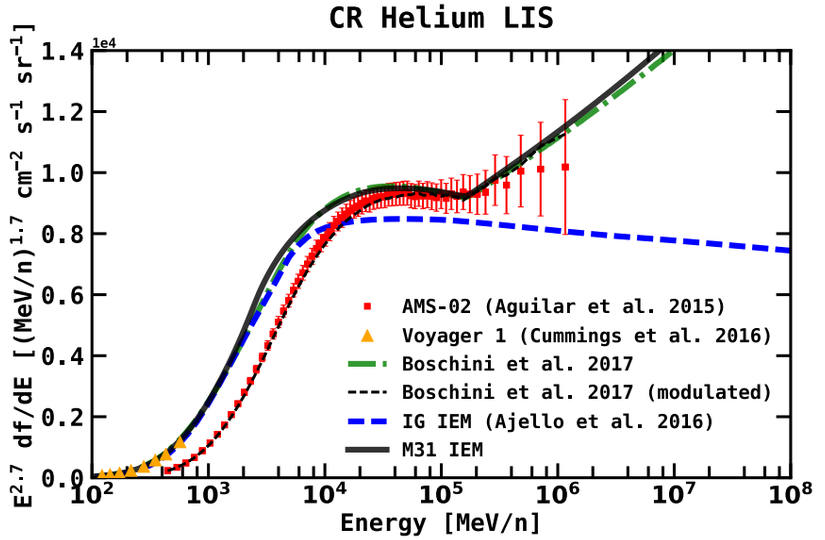


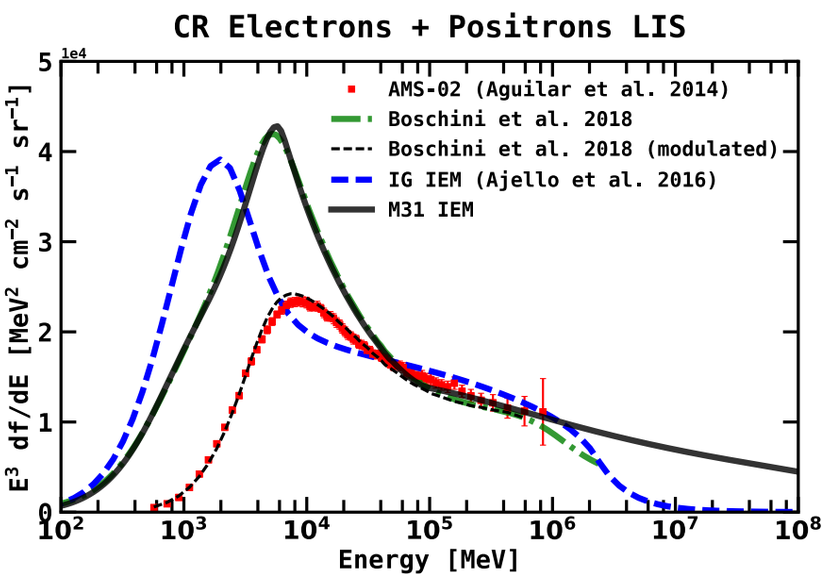


**Table 1**
GALPROP Model Parameters

| Parameter | M31 IEM | IG IEM |
|---|---|---|
| [a] $z$ [kpc] | 4 | 6 |
| [a] $r$ [kpc] | 20 | 30 |
| [b] $a$ | 1.5 | 1.64 |
| [b] $b$ | 3.5 | 4.01 |
| [b] $r_1$ | 0.0 | 0.55 |
| [c] $D_0$ [$10^{28}$ cm$^2$ s$^{-1}$] | 4.3 | 7.87 |
| [c] $\delta$ | 0.395 | 0.33 |
| [c] $\eta$ | 0.91 | 1.0 |
| [c] Alfvén speed, $v_A$ [km s$^{-1}$] | 28.6 | 34.8 |
| [d] $v_{\rm conv,0}$ [km s$^{-1}$] | 12.4 | ··· |
| [d] $dv_{\rm conv}/dz$ [km s$^{-1}$ kpc$^{-1}$ ] | 10.2 | ··· |
| [e] $R_{p,0}$ [GV] | 7 | 11.6 |
| [e] $R_{p,1}$ [GV] | 360 | ··· |
| [e] $\gamma_{p,0}$ | 1.69 | 1.90 |
| [e] $\gamma_{p,1}$ | 2.44 | 2.39 |
| [e] $\gamma_{p,2}$ | 2.295 | ··· |
| [e] $R_{\rm He,0}$ [GV] | 7 | ··· |
| [e] $R_{\rm He,1}$ [GV] | 330 | ··· |
| [e] $\gamma_{\rm He,0}$ | 1.71 | ··· |
| [e] $\gamma_{\rm He,1}$ | 2.38 | ··· |
| [e] $\gamma_{\rm He,2}$ | 2.21 | ··· |
| [e] $R_{e,0}$ [GV] | 0.19 | ··· |
| [e] $R_{e,1}$ [GV] | 6 | 2.18 |
| [e] $R_{e,2}$ [GV] | 95 | 2171.7 |
| [e] $\gamma_{e,0}$ | 2.57 | ··· |
| [e] $\gamma_{e,1}$ | 1.40 | 1.6 |
| [e] $\gamma_{e,2}$ | 2.80 | 2.43 |
| [e] $\gamma_{e,3}$ | 2.40 | 4.0 |
| [f] $J_p$ [$10^{-9}$ cm$^{-2}$ s$^{-1}$ sr$^{-1}$ MeV$^{-1}$] | 4.63 | 4.0 |
| [f] $J_e$ [$10^{-11}$ cm$^{-2}$ s$^{-1}$ sr$^{-1}$ MeV$^{-1}$] | 1.44 | 0.011 |
| [g] A5 [kpc] | 8–10 | 8–10 |
| [g] A6 [kpc] | 10–11.5 | 10–50 |
| [g] A7 [kpc] | 11.5–16.5 | ··· |
| [g] A8 [kpc] | 16.5–50 | ··· |
| [h] IC Formalism | Anisotropic | Isotropic |

**Note**. — For reference, we also give corresponding values for the ("Yusifov") IEMs used in Ajello et al. (2016) for the analysis of the inner Galaxy (IG).

[a] Halo geometry: $z$ is the height above the Galactic plane, and $r$ is the radius.

[b] CR source density. The parameters correspond to Eq. (1).

[c] Diffusion: $D(R) \propto \beta^\eta R^\delta$. $D(R)$ is normalized to $D_0$ at 4.5 GV.

[d] Convection: $v_{\rm conv}(z) = v_{\rm conv,0} + (dv_{\rm conv}/dz)z$.

[e] Injection spectra: The spectral shape of the injection spectrum is the same for all CR nuclei except for protons. The parameters correspond to Eq. (2).

[f] The proton and electron flux are normalized at the Solar location at a kinetic energy of 100 GeV. Note that for the IG IEM the electron normalization is at a kinetic energy of 25 GeV.

[g] Boundaries for the annuli which define the IEM. Only A5 (local annulus) and beyond contribute to the foreground emission for FM31.

[h] Formalism for the inverse Compton (IC) component.

## Source Density (top) and Injection Spectrum (bottom)

$$\rho(r) = \left(\frac{r + r_1}{r_\odot + r_1}\right)^a \times \exp\left(-b \times \frac{r - r_\odot}{r_\odot + r_1}\right)$$

$$q(R) \propto (R/R_0)^{-\gamma_0} \prod_{i=0}^{2} \left[1 + (R/R_i)^{\frac{\gamma_i - \gamma_{i+1}}{s_i}}\right]^{s_i}$$

- GALPROP-based (v56) combined diffusion-convection-reacceleration model with a uniform spatial diffusion coefficient and a single power law index over the entire rigidity range.
- Injection and diffusion parameters are derived from local CR measurements, including AMS-02 and Voyager 1.
- Use the GALPROP parameters from Boschini et al. 2017,2018, which employ GALPROP and HelMod.
- CR source density based on the distribution of pulsars.
- IG IEM from Ajello et al. 2016 used as a reference model in our study of the systematics for the M31 field.

# Interstellar Emission Model

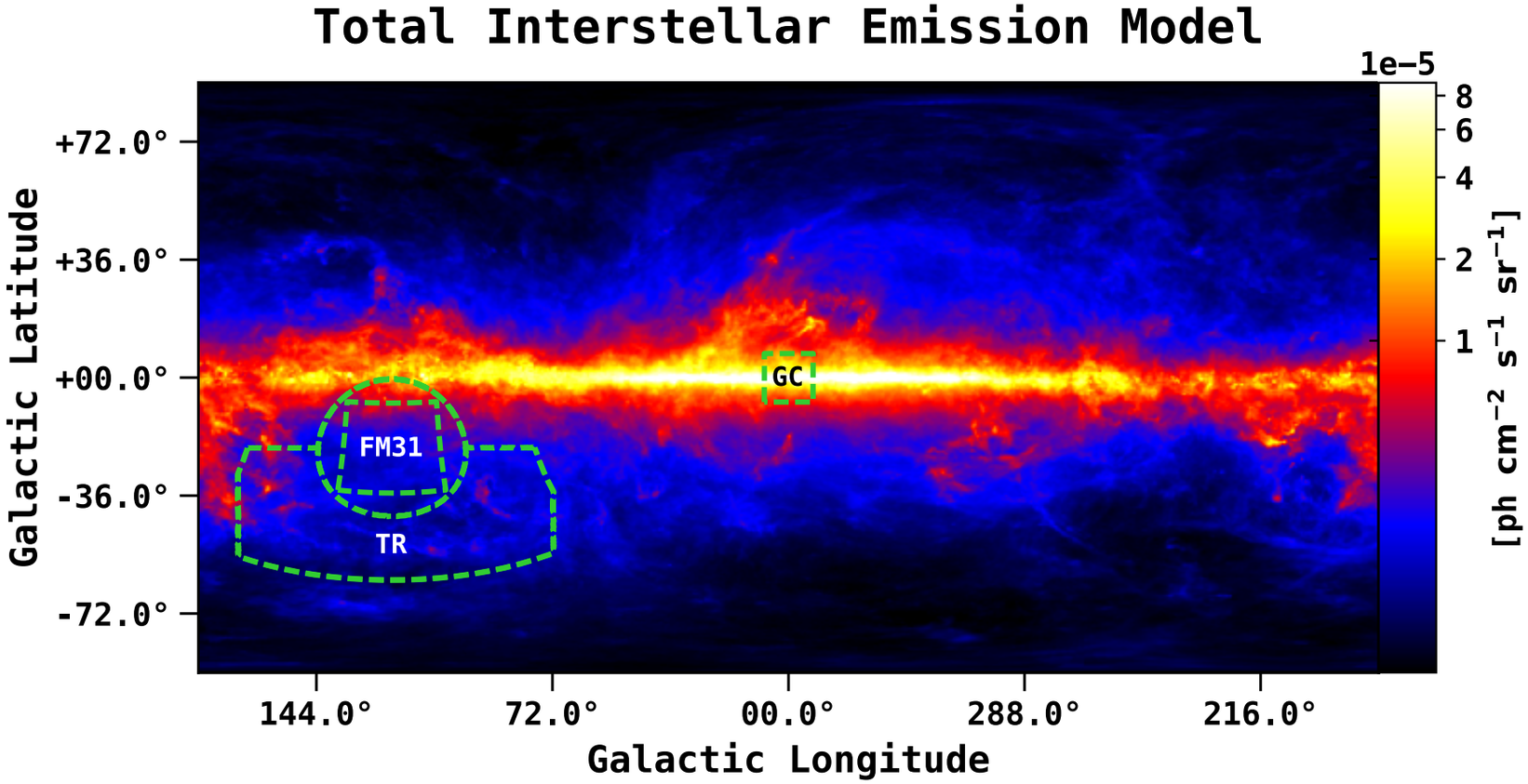


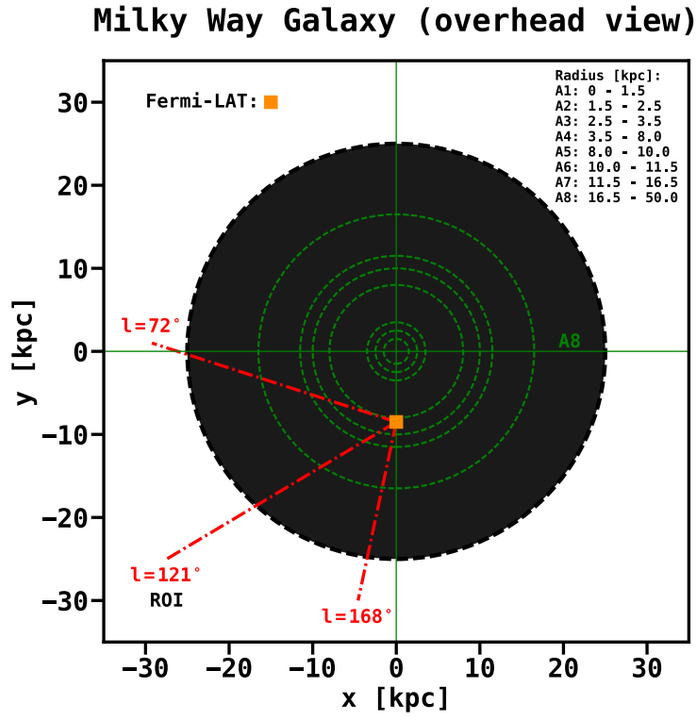


**Gas is placed at Galactocentric radii based on Doppler shifted emission and Galactic rotational models (Ackerman et al 2012):**

$$v_{\mathrm{LSR}} = R_{\odot}\left(\frac{V(R)}{R} - \frac{V_{\odot}}{R_{\odot}}\right)\sin(l)\cos(b).$$

- Total IEM for the MW integrated between 1-100 GeV.
- The color corresponds to the intensity and is shown in log scale. The intensity level corresponds to the initial GALPROP output, before tuning to the gamma-ray data.
- IEM has contributions from pi-0 decay, (anisotropic) IC emission, and Bremsstrahlung emission (see next slide).
- IEM is defined in Galactocentric annuli (A1-A8), but only A5-A8 contribute to the foreground emission towards M31.
- The green dashed circle corresponds to M31's virial radius. Our primary field of interest, FM31, lies within the virial radius, and we use the region outside (and below latitudes of -21.5°) as a tuning region (TR).
- For reference we also show the GC region, which corresponds to a 15° x 15° square centered at the GC.

# Interstellar Emission Model

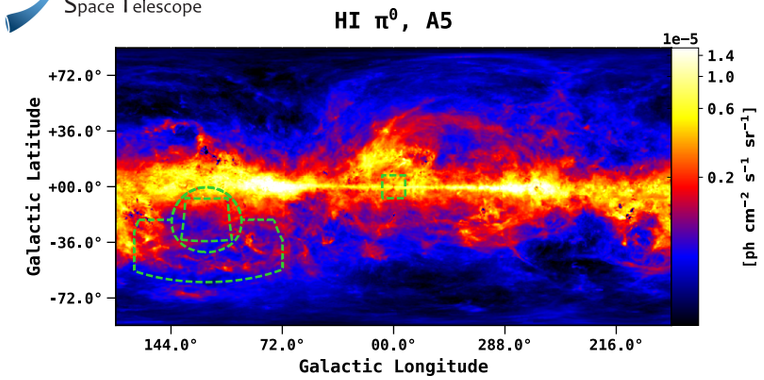


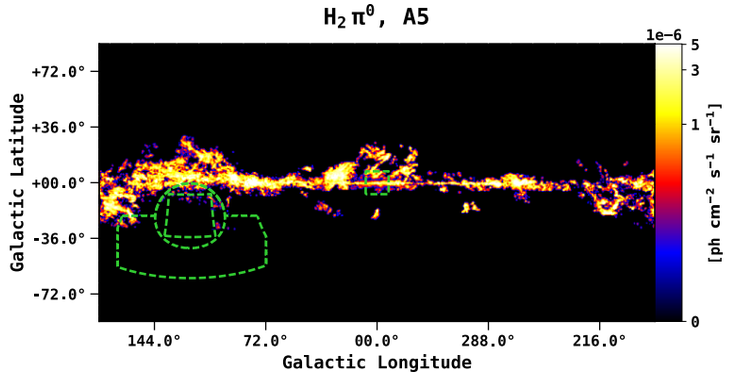


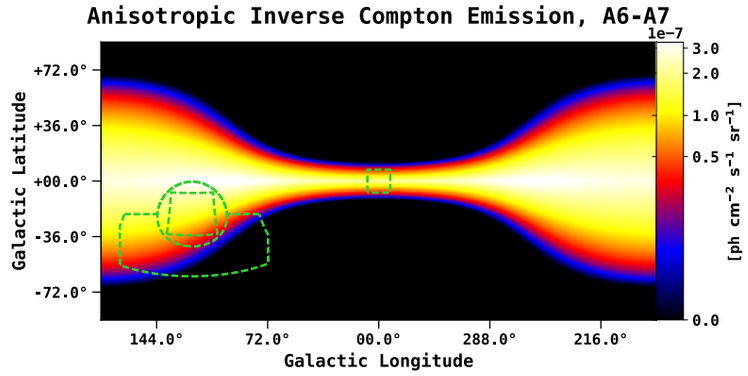


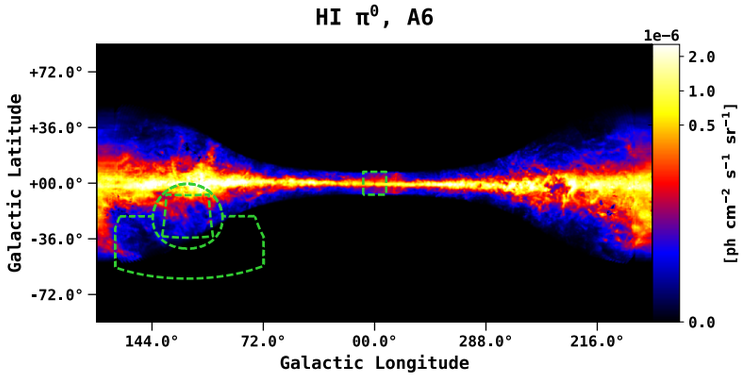


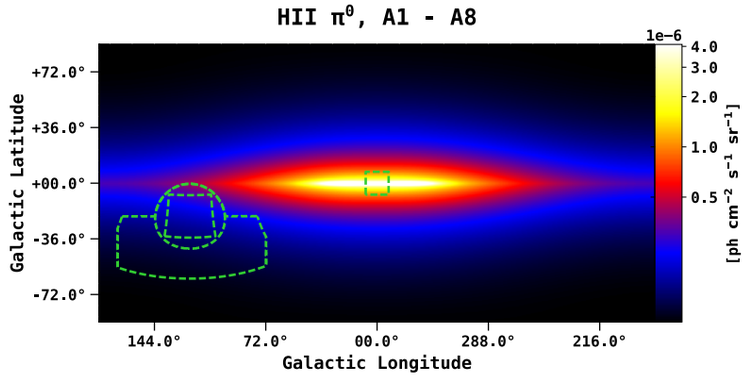


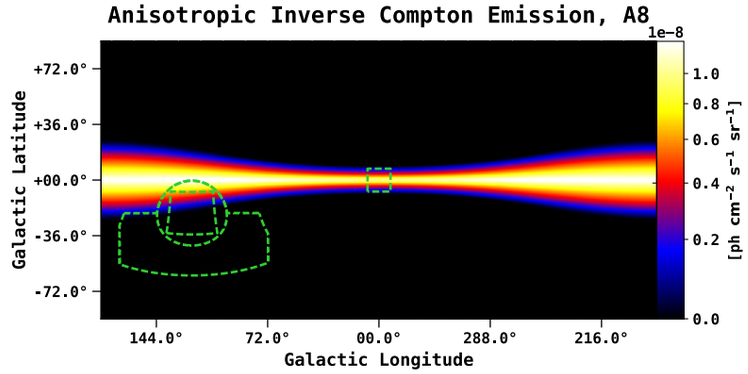


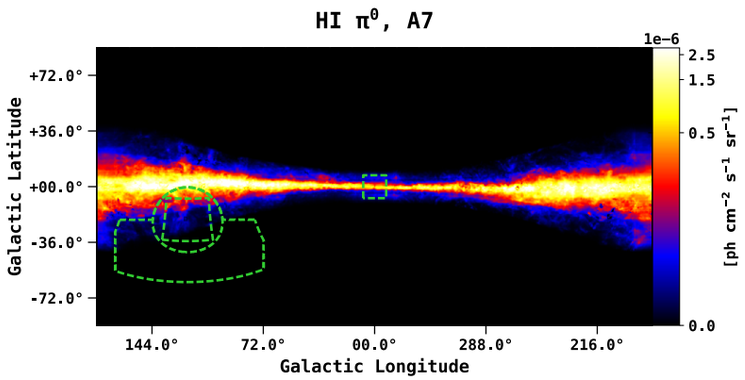


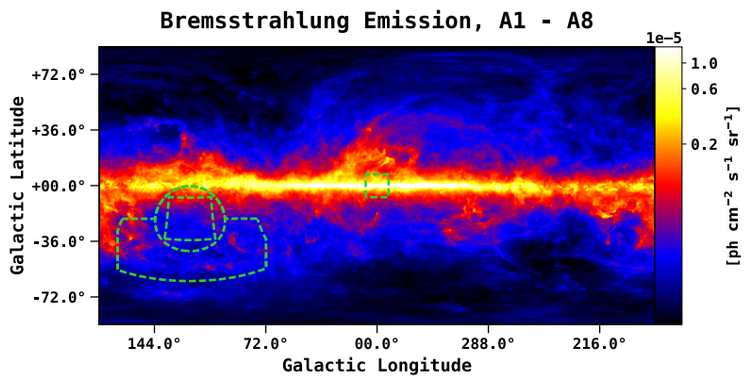


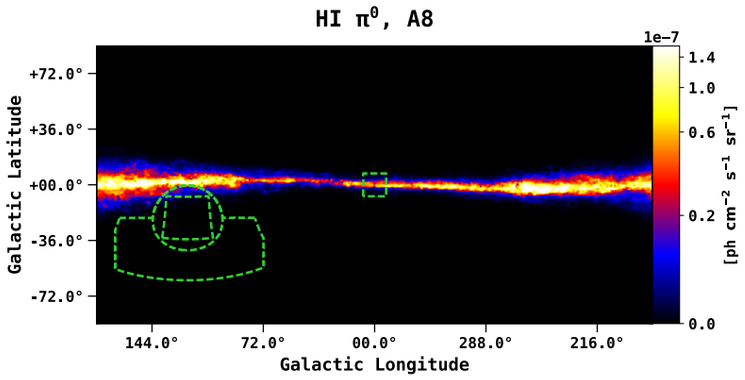


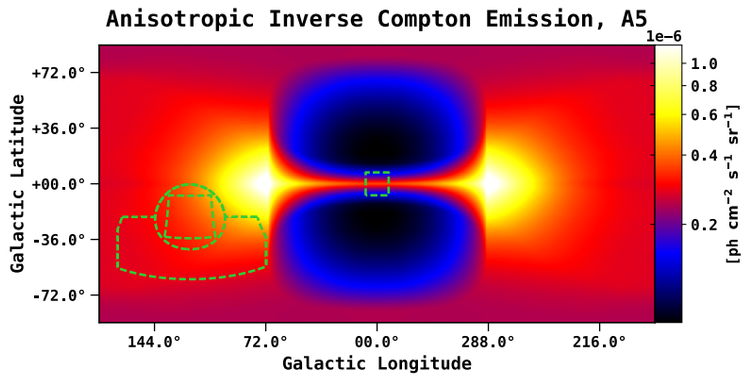


- FM31 has a significant contribution from emission related to H I gas, but there is very little contribution for H2 gas.
- H I map GALPROP employs is based on LAB+GASS data, which for our ROI corresponds to LAB data only.
- A uniform spin temperature of 150 K is assumed.
- Our model also accounts for the dark neutral medium.
- The distribution of He in the interstellar gas is assumed to follow that of hydrogen, with a He/H ratio of 0.11 by number.
- Anisotropic formalism used for IC calculation.
- H I A5 and IC A5 are the dominant contributions in FM31 below ~5 GeV.
- IC A8 has minor contribution towards top of the field.

# Isotropic Component

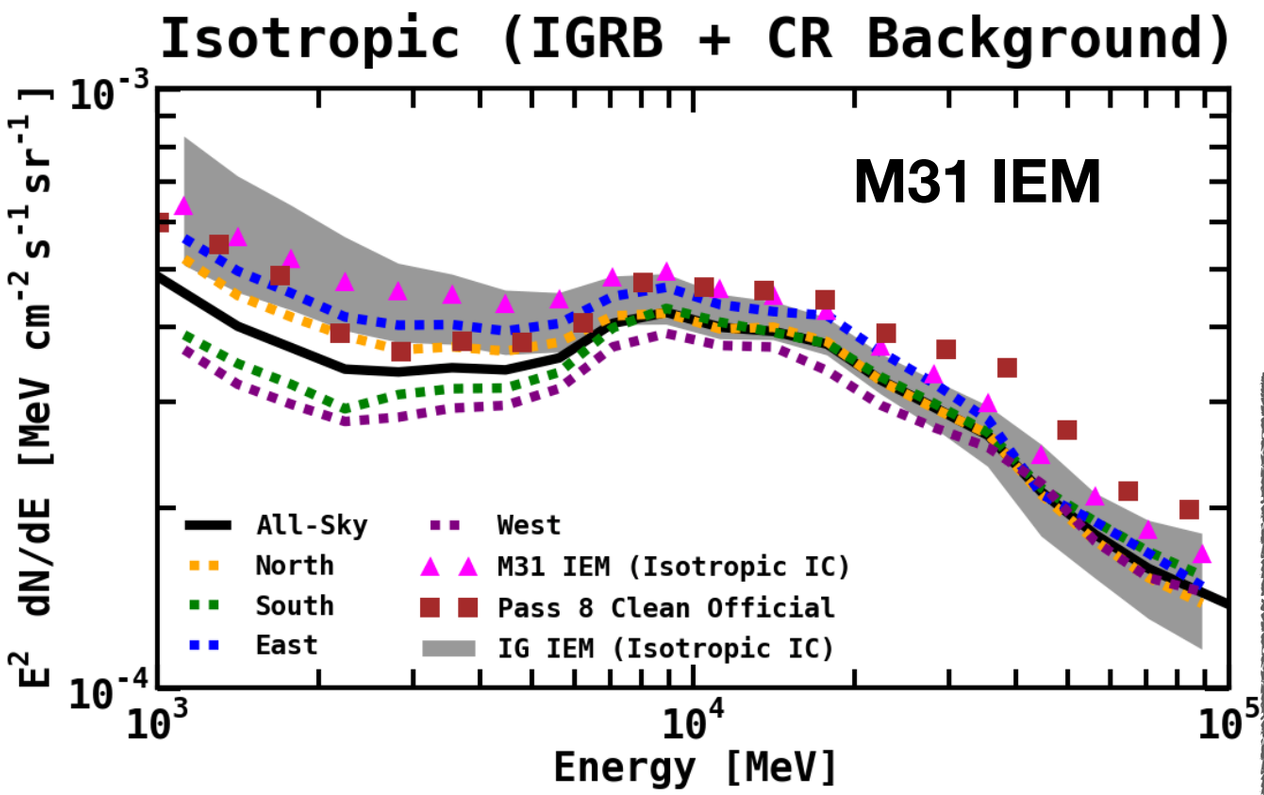


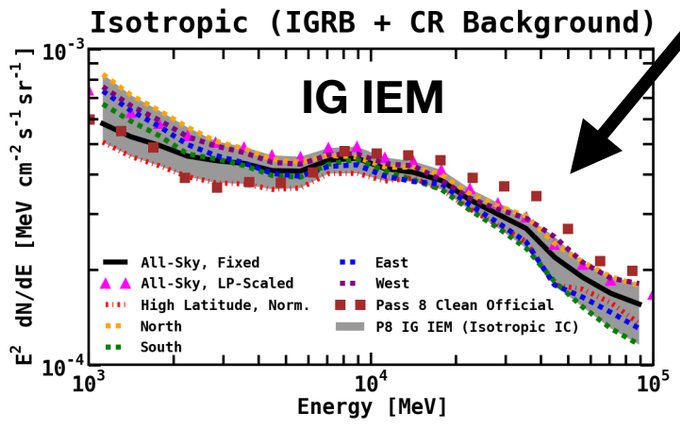


Isotropic Calculation for IG IEM, corresponding to the gray band in the bigger figure.

**Table 2**
Normalizations for Calculations of the Isotropic Component **(M31 IEM)**

| Region | $\pi^0$ | AIC |
|---|---|---|
| All-sky | $1.319 \pm 0.005$ | $1.55 \pm 0.04$ |
| North | $1.430 \pm 0.010$ | $1.14 \pm 0.05$ |
| South | $1.284 \pm 0.006$ | $1.86 \pm 0.05$ |
| East | $1.397 \pm 0.009$ | $1.07 \pm 0.05$ |
| West | $1.287 \pm 0.006$ | $1.88 \pm 0.05$ |

- We use the "all-sky" isotropic spectrum.
- Fit includes 3FGL sources fixed, sun and moon templates fixed, Wolleben component, all-sky pi-0 decay and IC normalization scaled, and all-sky Bremsstrahlung fixed (see above table).
- Note that regardless of the fit variation, the spectrum of the isotropic contains a bump near ~10 GeV.

## Systematic checks for the isotropic component:

- **The spectrum is calculated self-consistently with the M31 IEM**.
- **The normalization is determined in the TR**: 1.06 +/- 0.04. This remains fixed for all fits in FM31.
- **We repeat the analysis using the IG IEM, which has its own self-consistently derived isotropic component.** In this case the isotropic spectrum is determined at high latitudes, and the normalization remains fixed to its nominal value (1.0) for the fits in FM31.
- **We also repeat the analysis with the FSSC IEM and corresponding isotropic spectrum.** For this variation we use an extended energy range of 300 MeV - 300 GeV. The normalization of the isotropic component is fit in FM31 (along with the Galactic diffuse and point sources). The best-fit normalization is found to be 1.04 +/- 0.005.
- Using the FSSC IEM, **we repeat the analysis using both the Clean and UltraCleanVeto selection**.
- Although the residual emission in FM31 is found to be (very) roughly uniformly distributed over the entire field, **the residual emission in FM31 is not found to be isotropic**.

# Tuning the IEM

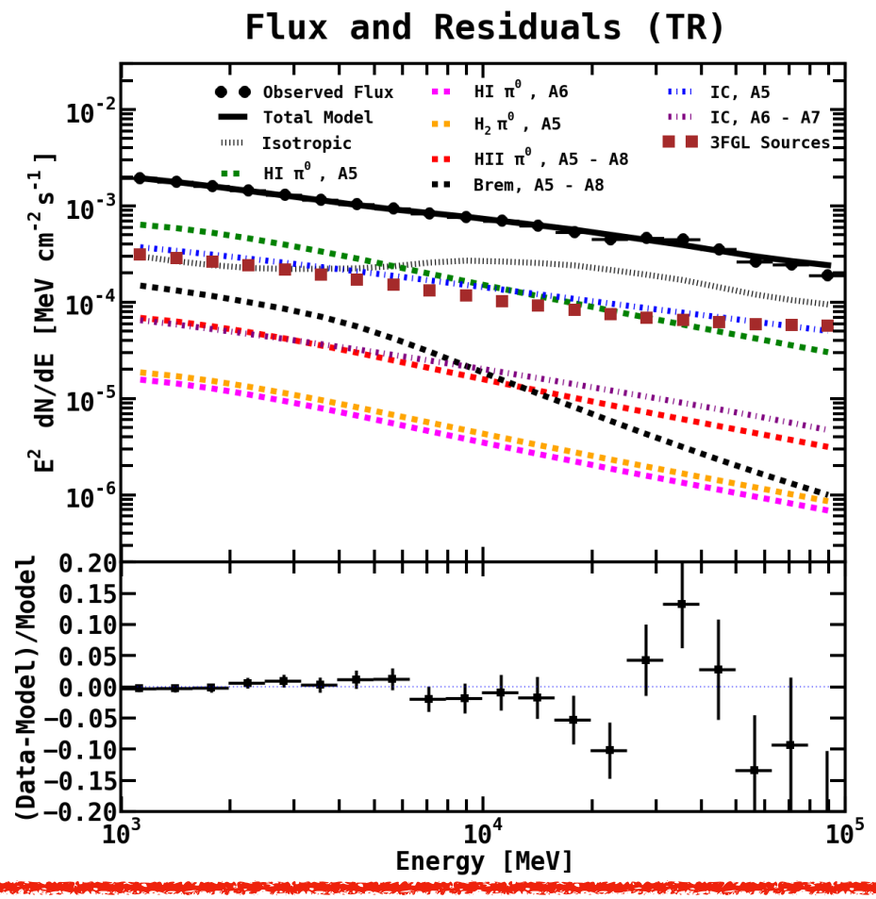


**Table 3**
Baseline Values for the IEM Components in the TR

| Component | Normalization | Flux ($\times 10^{-9}$) (ph cm$^{-2}$ s$^{-1}$) | Intensity ($\times 10^{-8}$) (ph cm$^{-2}$ s$^{-1}$ sr$^{-1}$) |
|---|---|---|---|
| H I $\pi^0$, A5 | $1.10 \pm 0.03$ | $439.4 \pm 11.0$ | $153.1 \pm 3.8$ |
| H I $\pi^0$, A6 | $5.0 \pm 1.3$ | $10.6 \pm 2.8$ | $3.7 \pm 1.0$ |
| $H_2$ $\pi^0$, A5 | $2.1 \pm 0.1$ | $12.6 \pm 0.7$ | $4.4 \pm 0.3$ |
| Bremsstrahlung | $1.0 \pm 0.6$ | $100.4 \pm 58.3$ | $35.0 \pm 20.3$ |
| IC, A5 | $2.3 \pm 0.1$ | $274.7 \pm 14.0$ | $95.7 \pm 4.9$ |
| IC, A6 – A7 | $3.5 \pm 0.4$ | $45.7 \pm 4.8$ | $15.9 \pm 1.7$ |
| Isotropic | $1.06 \pm 0.04$ | $248.1 \pm 10.4$ | $86.4 \pm 3.6$ |

**Note**. — The normalizations of the diffuse components are freely scaled, as well as all 3FGL sources in the region. The fit uses the all-sky isotropic spectrum. Intensities are calculated by using the total area of the TR, which is 0.287 sr.

## Results for the TR:

- Diffuse components listed in the table are scaled in the fit.
- **Isotropic possesses a normalization of 1.06 +/- 0.04**, which remains fixed for all fits in FM31.
- **Bremsstrahlung possesses a normalization of 1.0 +/- 0.6**, which also remains fixed for all fits in FM31.
- 3FGL sources in the TR are also scaled in the fit, but they do not significantly impact the normalizations of the diffuse components.
- **The model describes the data well across all energies and over the entire region**.
- Residuals worsen at higher energies, but still consistent with statistical fluctuations. Possibly related to poorly modeled 3FGL spectra. We note that it's also possible that the IEM may be compensating for an un-modeled component, i.e. a MW halo component.
- **Normalizations of diffuse components all within reasonable agreement with the GALPROP predictions** (note: IC A6-A7 is a bit high. Same for H I A6, but this component has very little contribution in the TR).

# Results for Baseline Fit in FM31

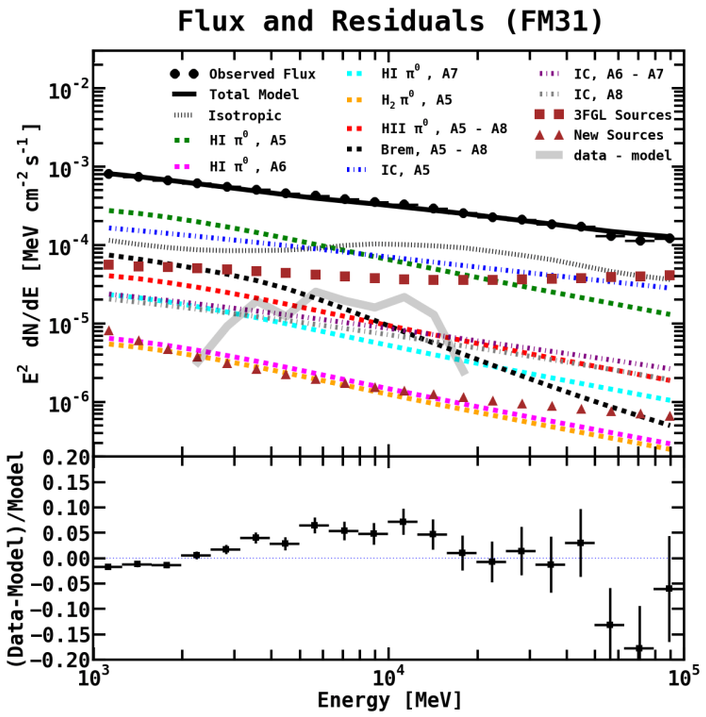


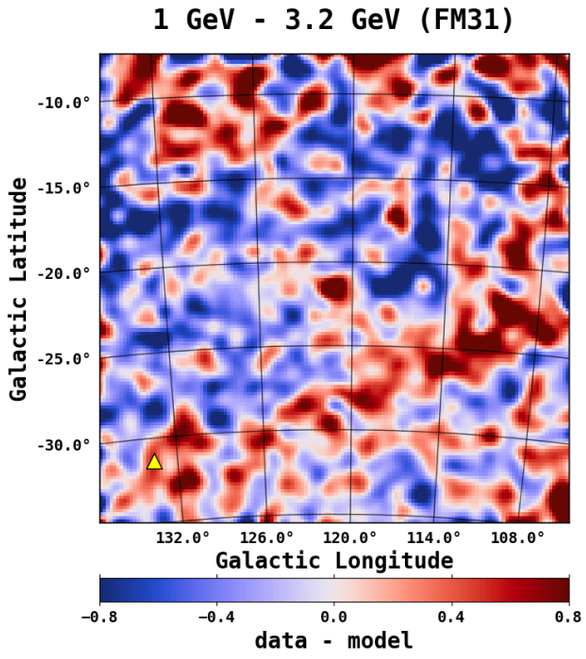


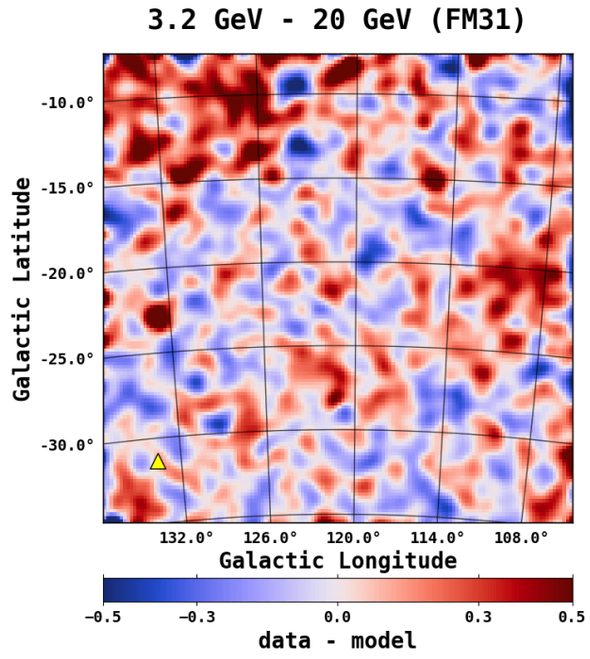


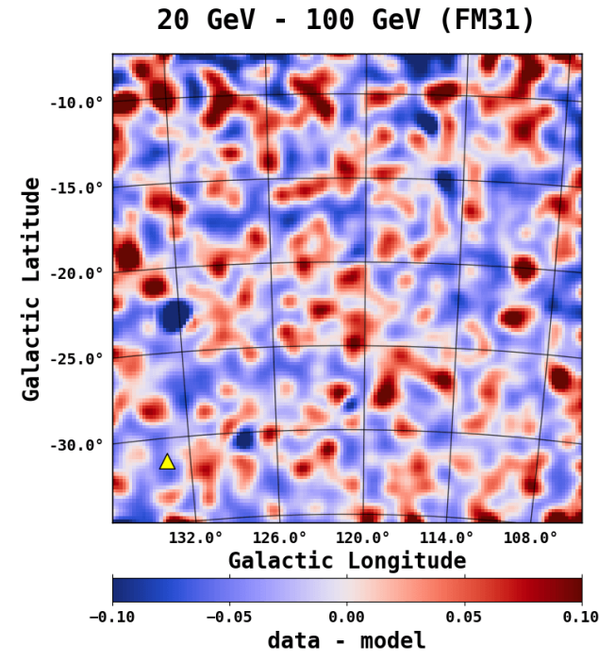


## Results for the Baseline Fit in FM31:

- Fit is performed by scaling the diffuse sources and point sources self-consistently.
- **Positive residual emission observed between ~3-20 GeV at the level of ~5%**.
- **Spatial residuals show structured excess and deficits**, primarily in the 1st energy bin. Residuals in the 2nd bin are more uniformly distributed, although structures can still be seen.
- **A large arc feature can be observed in the residuals**, beginning at the upper-left corner of the field, which then extends around to the projected position of M33 (shown with a yellow triangle).
- **Performed two primary variations of the initial baseline fit with the M31 IEM**: (1) fixed the normalizations of IC components to best-fit values obtained in the TR. (2) Freely scaled the IC components in FM31 along with the other diffuse components: similar results.
- **Rescaled the diffuse components in smaller subregions**: unable to flatten the residuals.
- **Allowed for a radial-dependent spectral variation in the H I components and IC components** by using a power law scaling: no change in the spectral shape, and unable to flatten residuals.

# Results for Baseline Fit in FM31

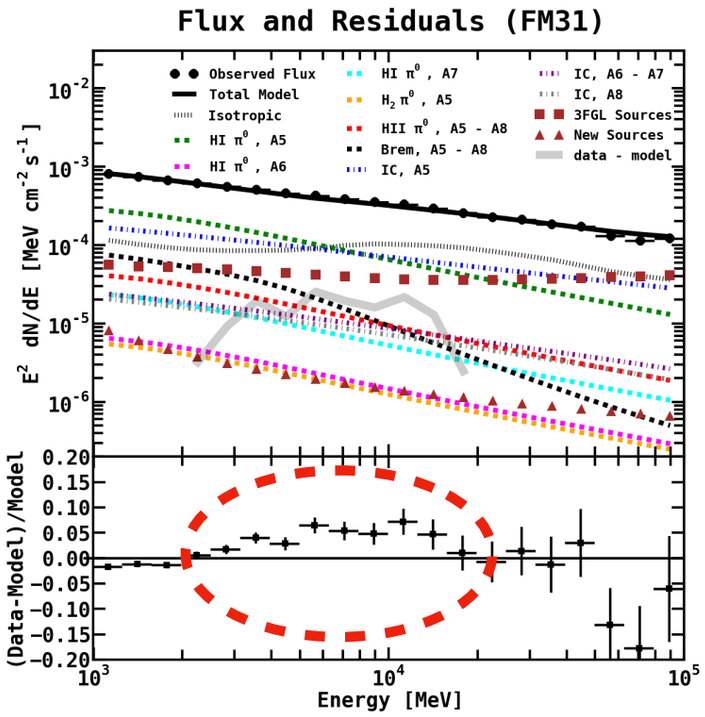


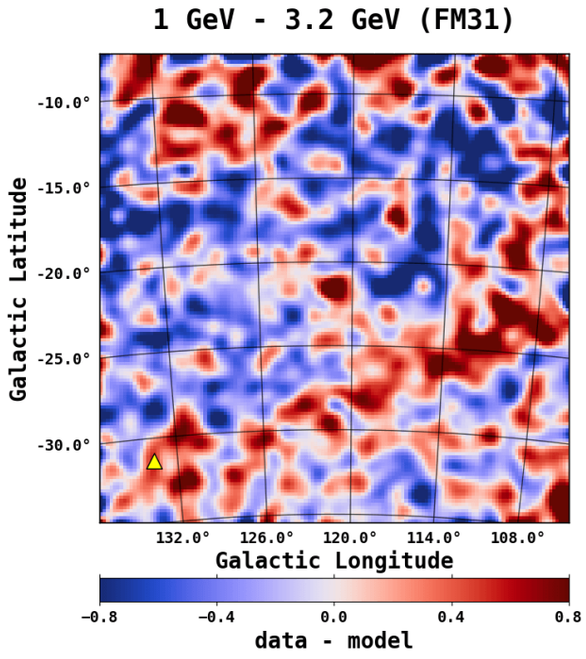


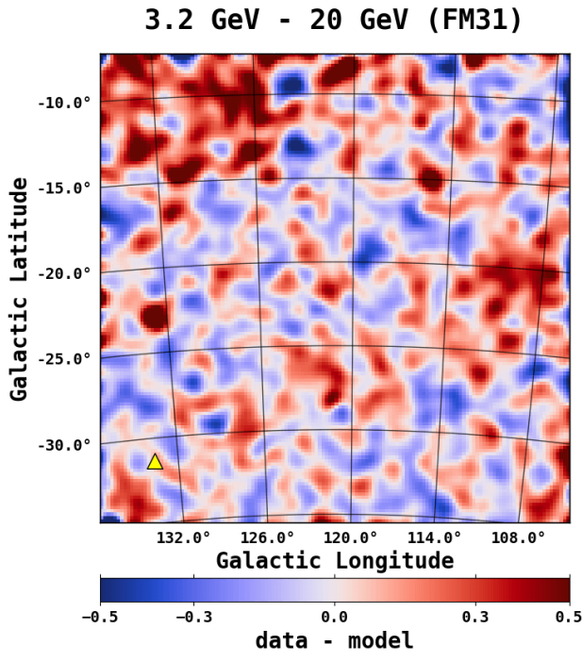


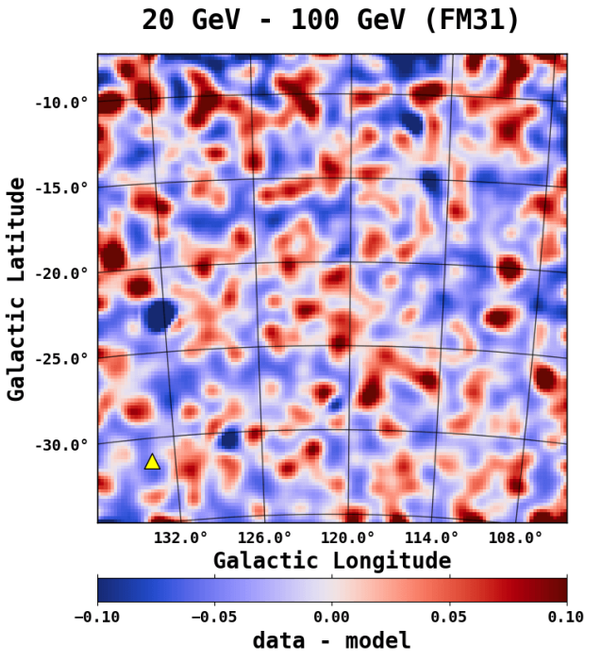


## Results for the Baseline Fit in FM31:

- Fit is performed by scaling the diffuse sources and point sources self-consistently.
- **Positive residual emission observed between ~3-20 GeV at the level of ~5%**.
- **Spatial residuals show structured excess and deficits**, primarily in the 1st energy bin. Residuals in the 2nd bin are more uniformly distributed, although structures can still be seen.
- **A large arc feature can be observed in the residuals**, beginning at the upper-left corner of the field, which then extends around to the projected position of M33 (shown with a yellow triangle).
- **Performed two primary variations of the initial baseline fit with the M31 IEM**: (1) fixed the normalizations of IC components to best-fit values obtained in the TR. (2) Freely scaled the IC components in FM31 along with the other diffuse components: similar results.
- **Rescaled the diffuse components in smaller subregions**: unable to flatten the residuals.
- **Allowed for a radial-dependent spectral variation in the H I components and IC components** by using a power law scaling: no change in the spectral shape, and unable to flatten residuals.

# Analysis of the H I-Related Emission

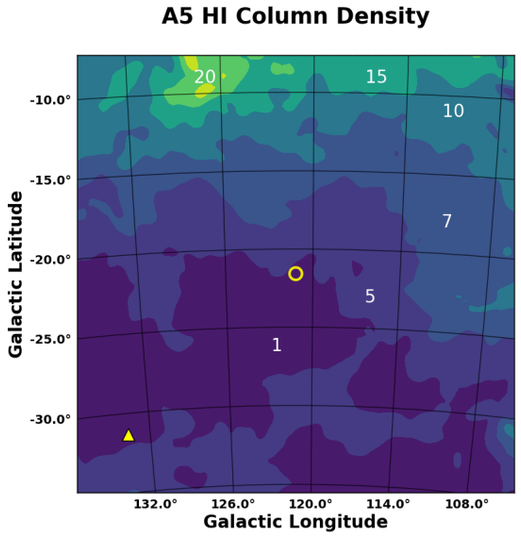


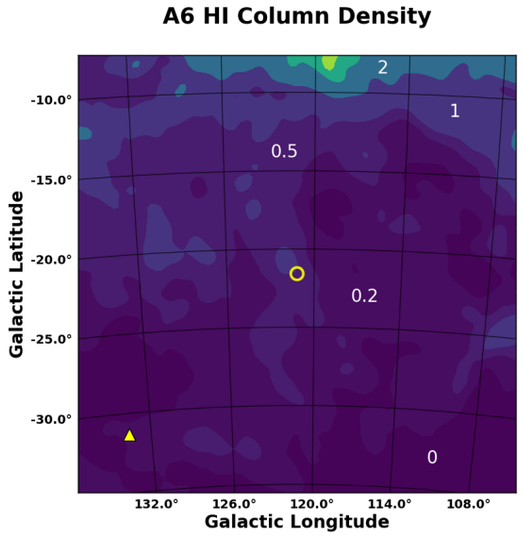


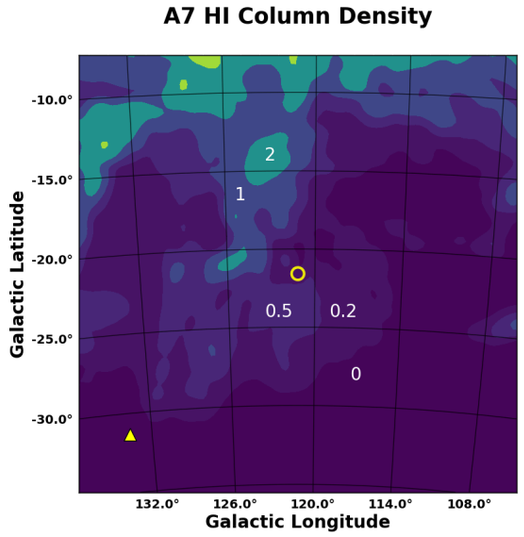


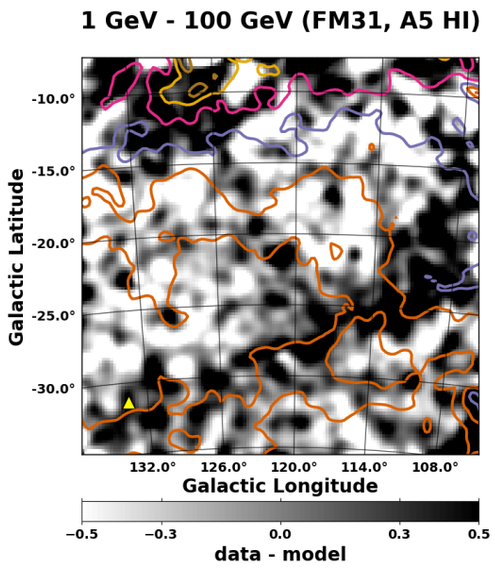


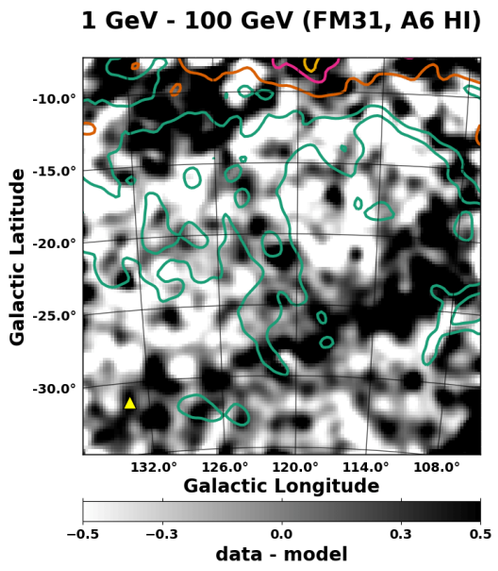


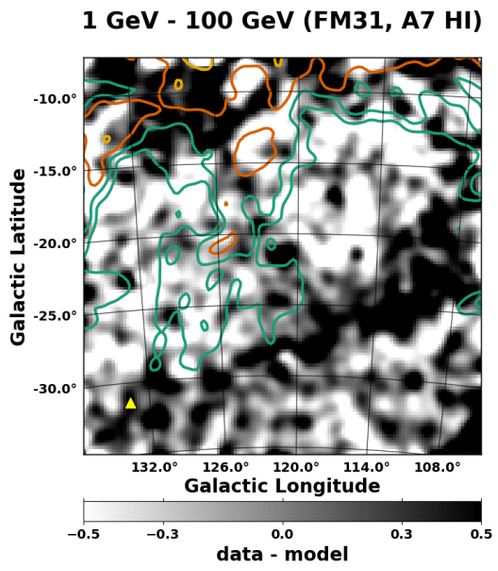


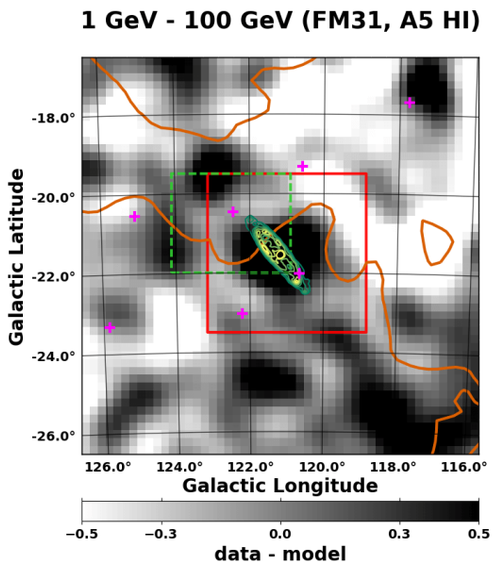


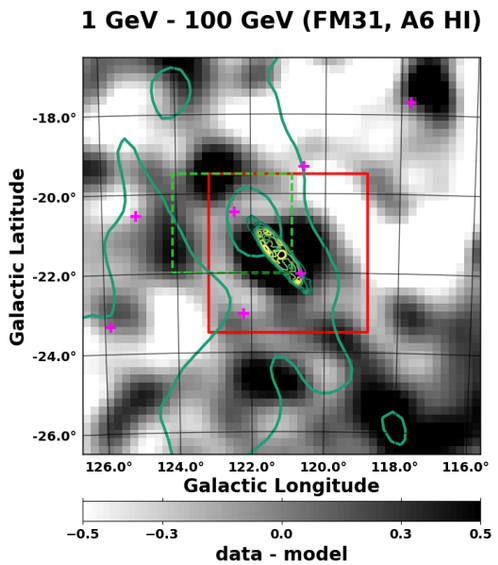


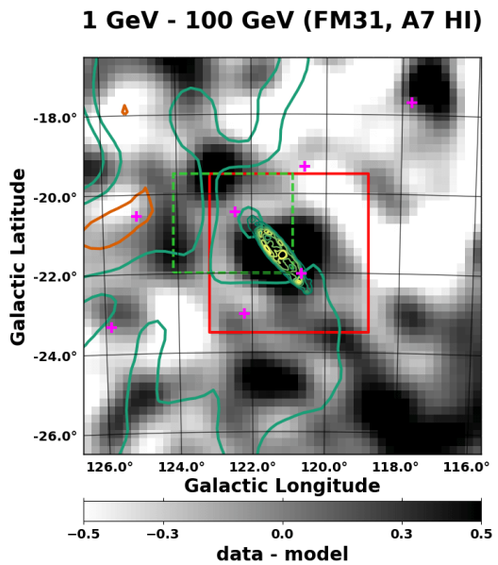


- Emission associated with the arc feature in the residuals is found to correlate with the local foreground H I column density.
- This may be an indication of a spatially varying spin temperature and/or inaccuracies in the modeling of the dark neutral medium (which is determined as part of an all-sky procedure).
- The H I column densities (A6 and A7) are found to be positionally coincident with the major axis of the M31 disk (the position angle of M31 is 38º).

# Analysis of the H I-Related Emission

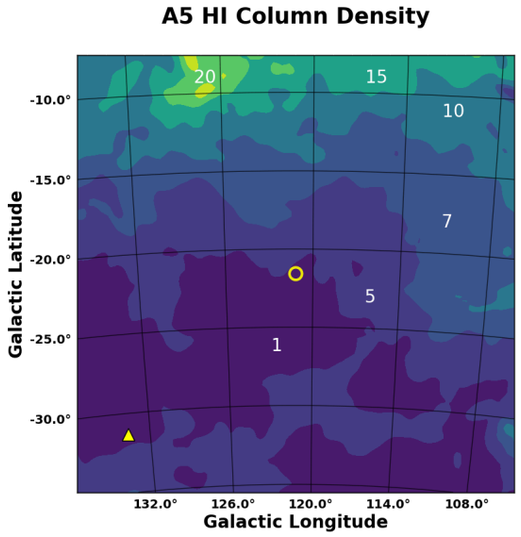


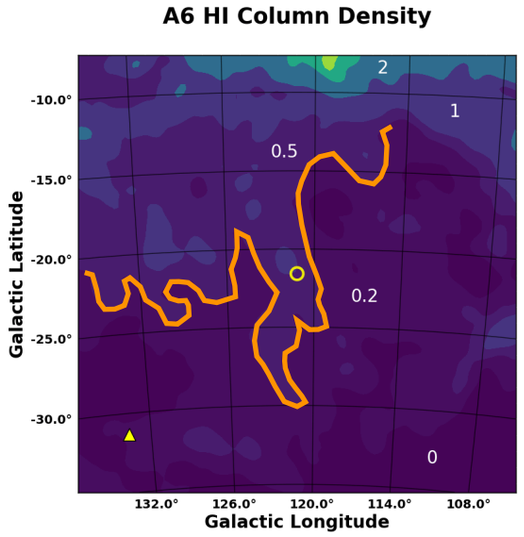


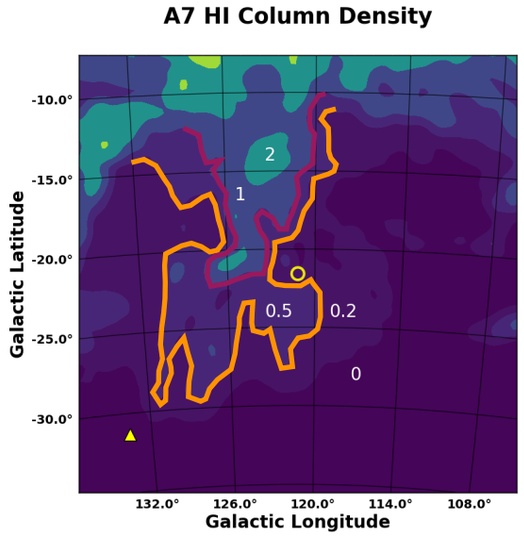


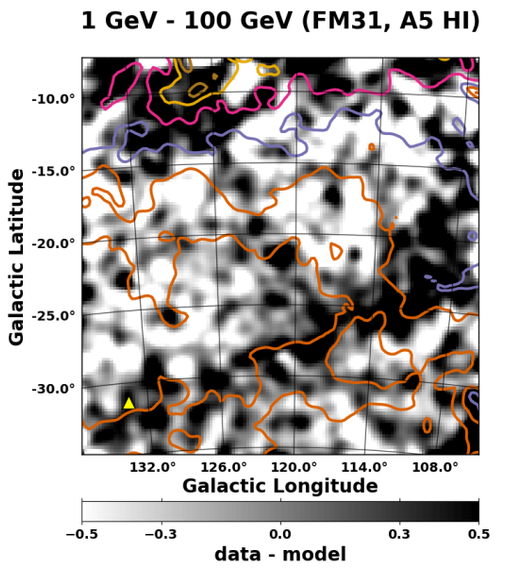


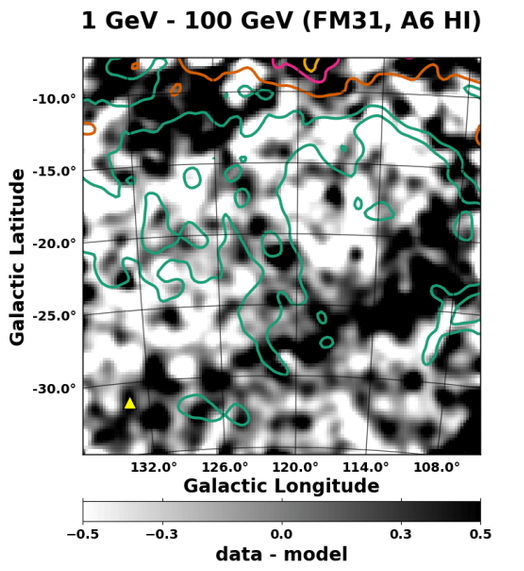


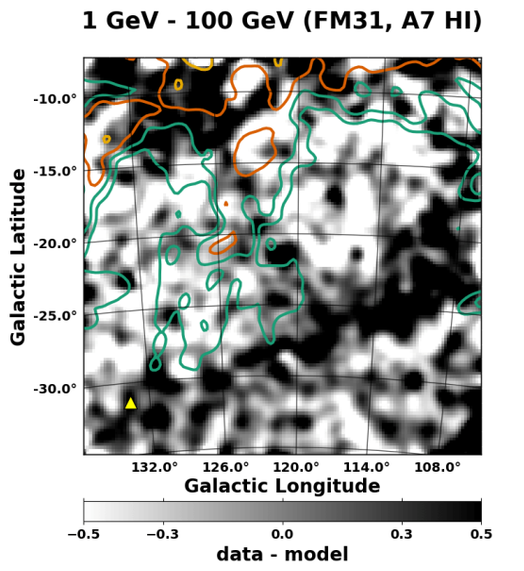


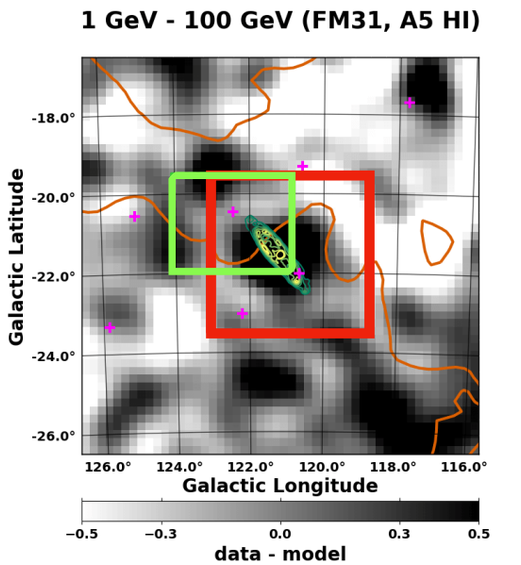


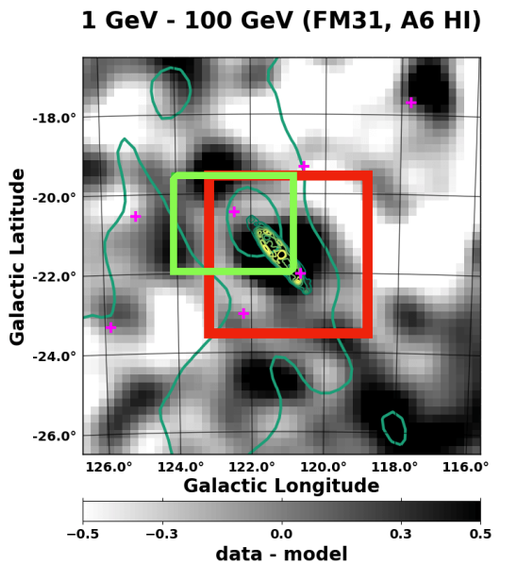


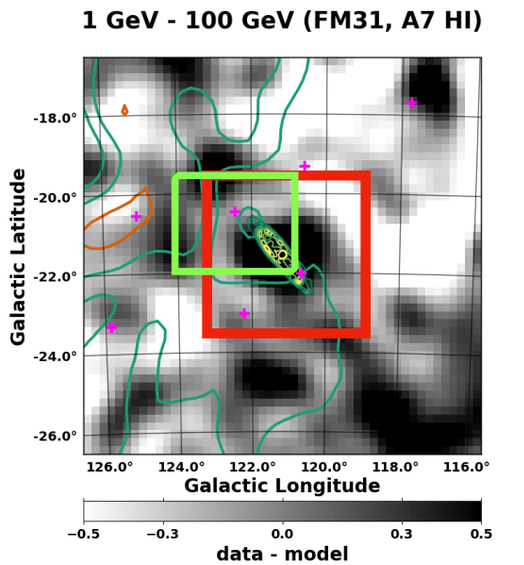


- Emission associated with the arc feature in the residuals is found to correlate with the local foreground H I column density.
- This may be an indication of a spatially varying spin temperature and/or inaccuracies in the modeling of the dark neutral medium (which is determined as part of an all-sky procedure).
- The H I column densities (A6 and A7) are found to be positionally coincident with the major axis of the M31 disk (the position angle of M31 is 38º).

# The Arc Template Fit

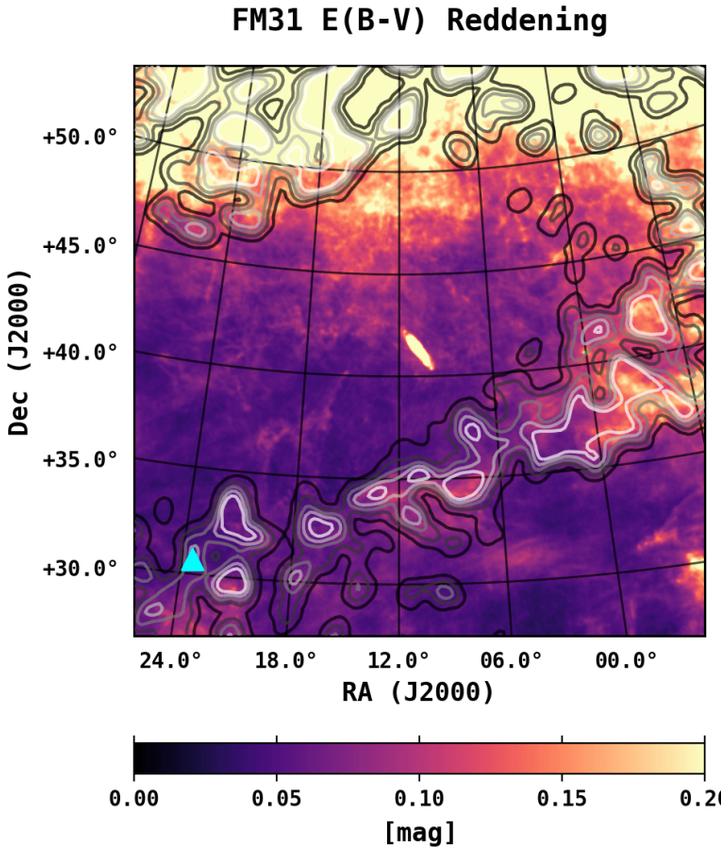


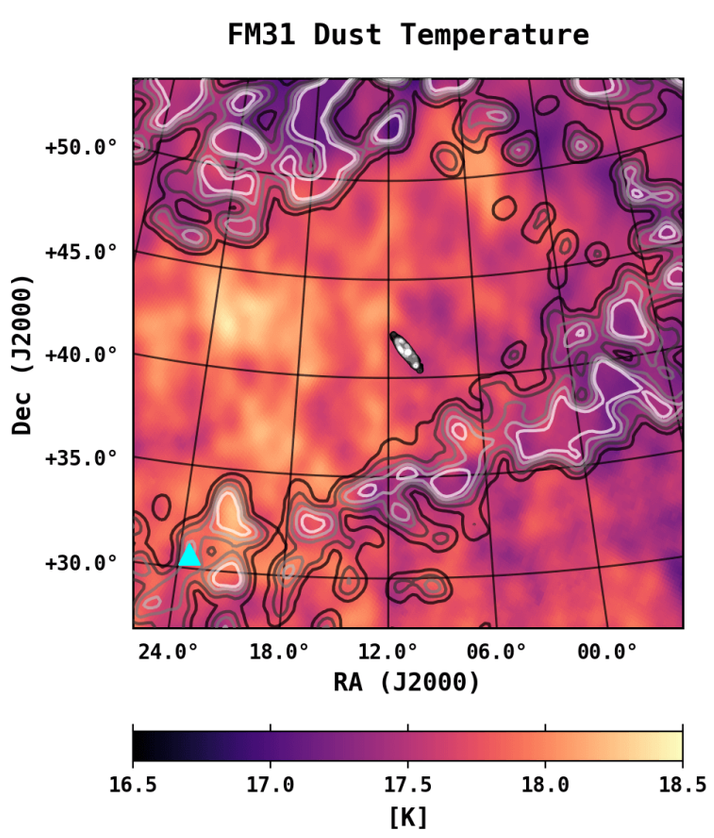


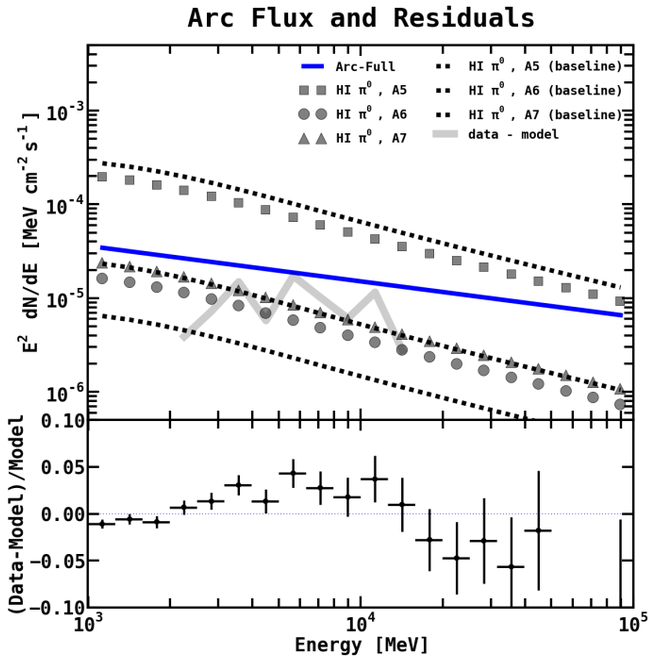


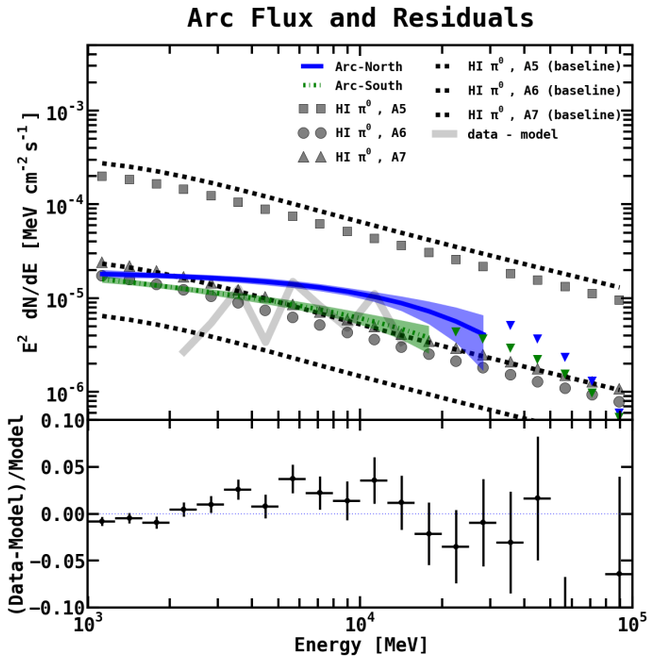


## Results for the Arc Fit:

- Emission associated with the arc feature in the residuals is also found to correlate with properties of the dust, including regions where the dust is relatively cold.
- **We construct a template for the arc emission by selecting the positive residual emission in FM31 that correlates with tracers of the foreground gas and dust. We refer to this as the arc template**.
- The arc is fit simultaneously with the other components.
- Tried five variations of the fit (we only show two): all give similar results. This includes using different spectral models and breaking the arc into smaller components.
- **The arc fit is unable to flatten the positive residual emission between ~3-20 GeV**.
- **The index of the arc emission has a value ~2.0-2.4,** notably flatter than the other gas-related emission in the field.
- **The arc emission is found to have a high-energy cutoff**.

# The Arc Template Fit

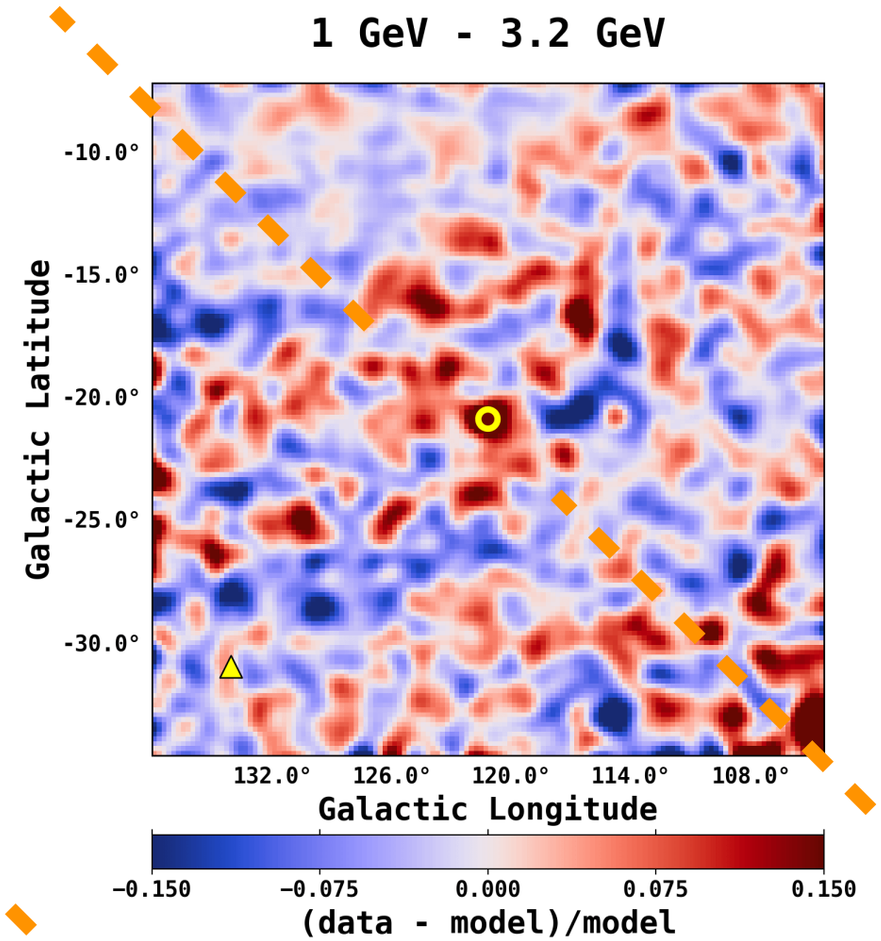


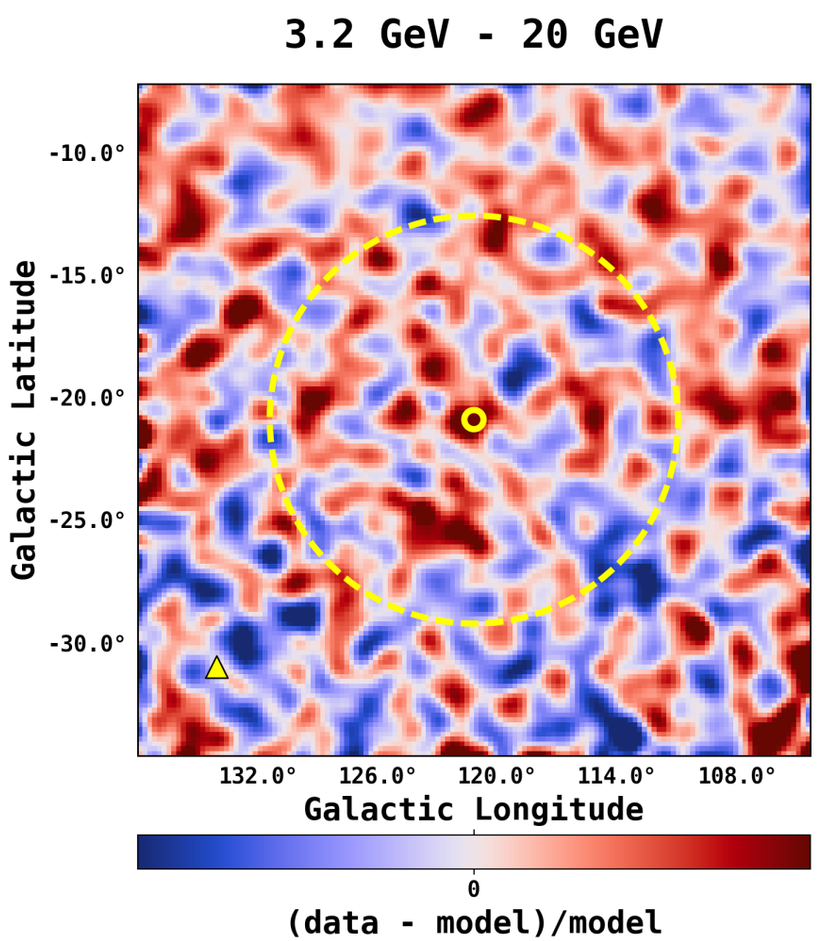


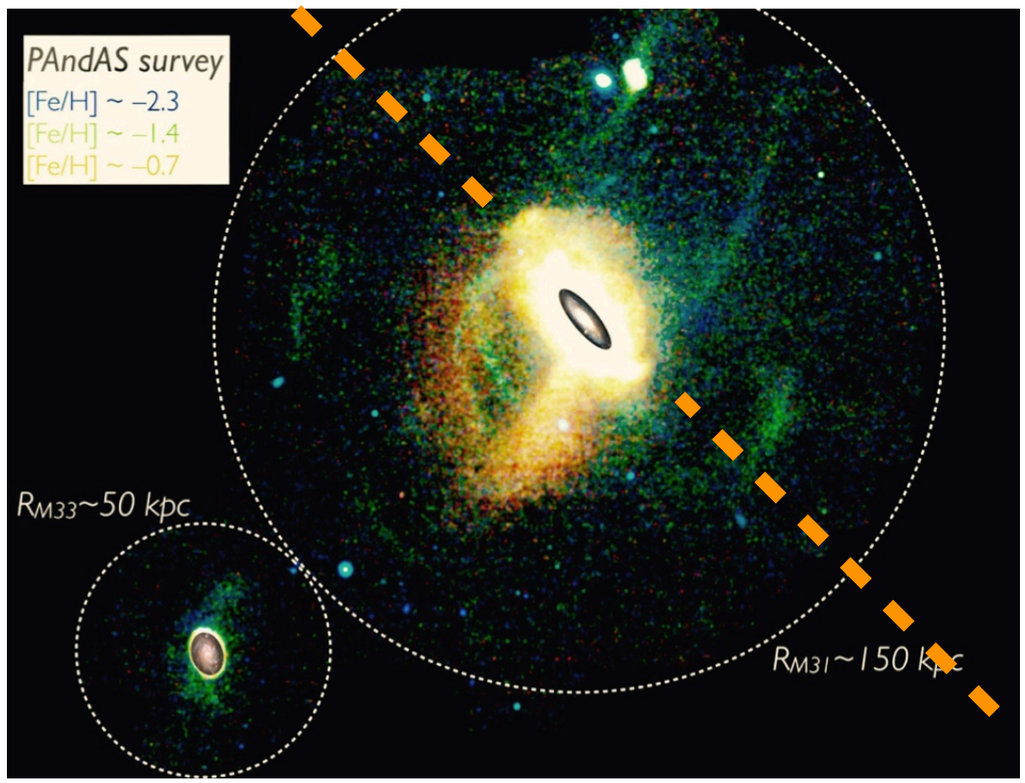


## Results for the Arc Fit:

- The arc feature no longer dominates the residuals, as expected.
- The first energy bin of the spatial residuals still shows structured excesses and deficits, possibly associated with the M31 system.
- The positive residual emission in the second energy bin, associated with the excess between ~3-20 GeV, appears **roughly** uniformly distributed over the field.

# Summary of the Excess for all IEMs

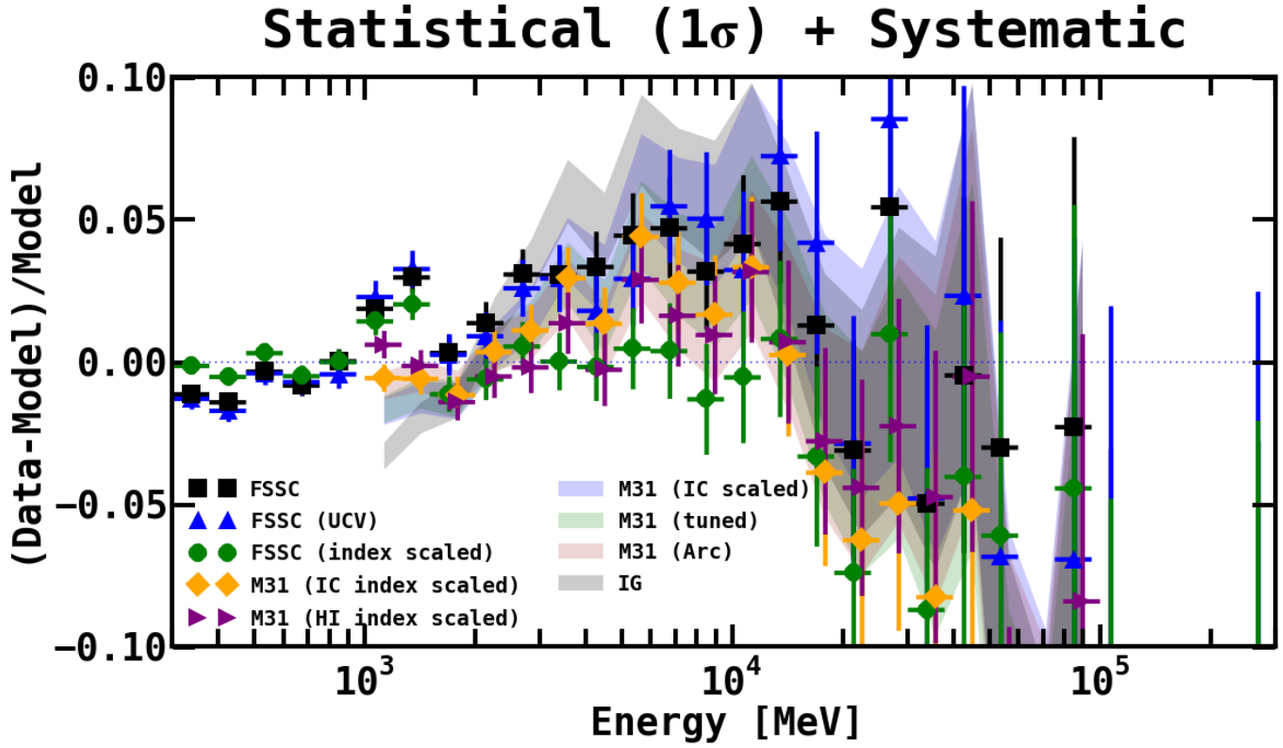


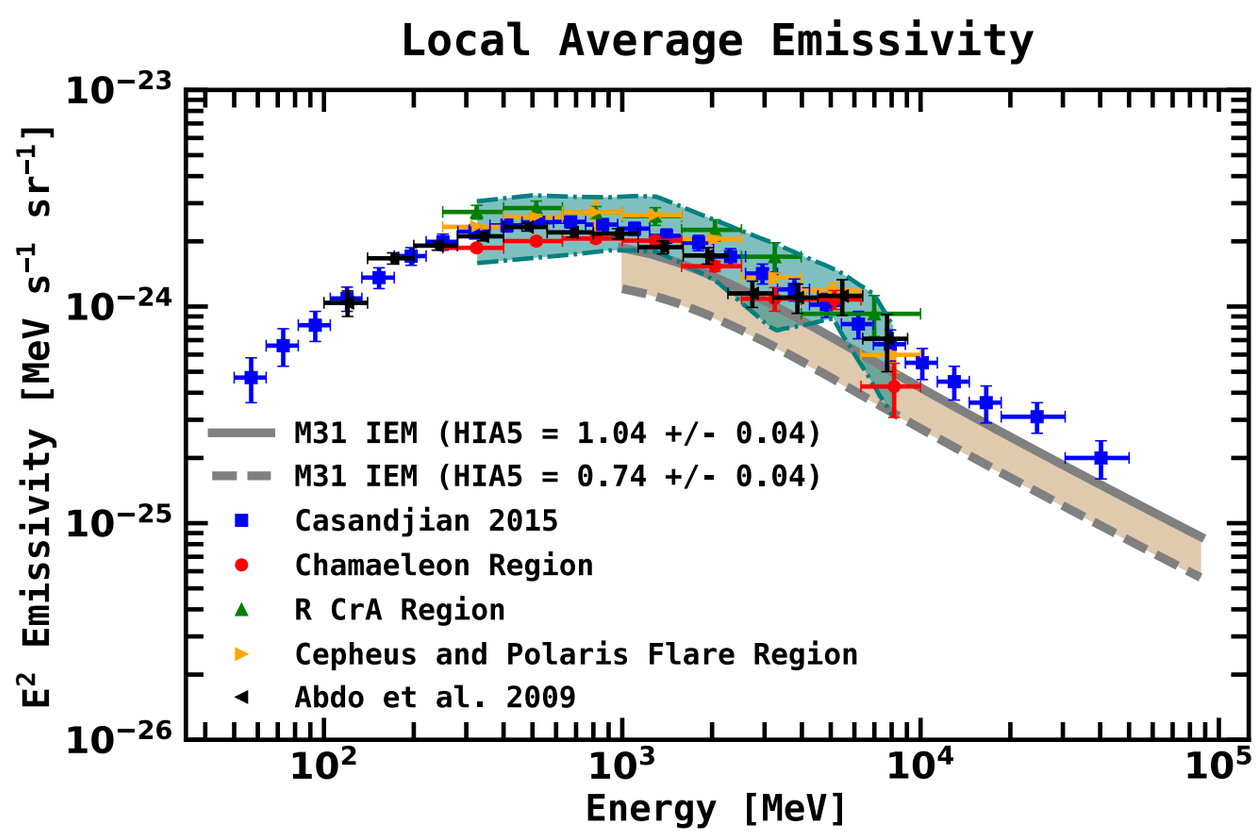


- We find evidence for a systematic excess between ~3-20 GeV at the level of 3-5%.
- There is only one case for which the signal can be flattened. This results from using the FSSC IEM (intended for point source analysis), and fitting both the Galactic diffuse component (including the index) and the isotropic component in the signal region.
- The FSSC IEM is not intended for extended source analysis, and this result illustrates how the application of an improper IEM for analysis of largely extended emission can alter the physical results. The M31 IEM is our benchmark model.
- The local average emissivity measured in FM31 is a bit low compared to other measurements (which may be expected given it's position at high latitude and away from the plane), but still consistent within one sigma.

# Adding M31-Related Components to the Model

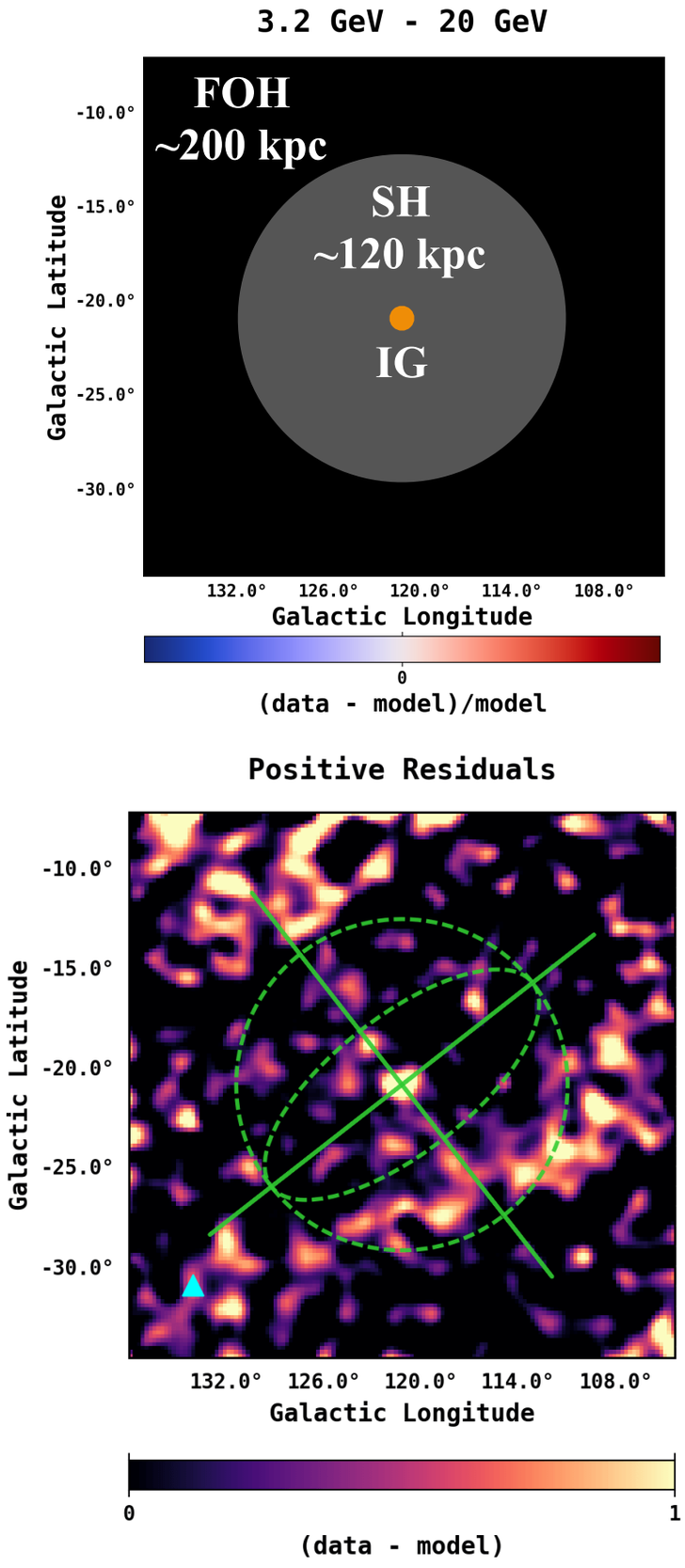


- Inner galaxy (IG): 0.4 degree disk, as determined from previous LAT analysis.
- Spherical halo (SH): extending out to a projected radius of ~120 kpc. Set by the geometry from the construction of the arc template. Also happens to enclose most of M31's globular cluster population, satellite population, and the M31 cloud.
- Far outer halo (FOH): covers remaining extent of the field. This component approaches the Galactic disk and suffers worst from Galactic confusion.
- Fit also includes arc template.

# Adding M31-Related Components to the Model

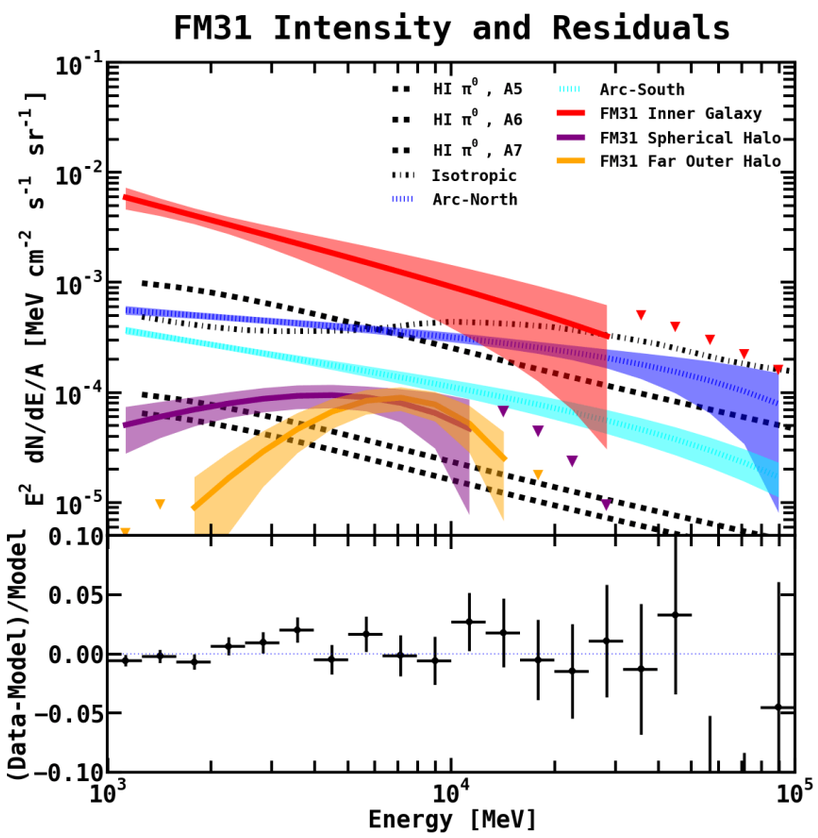


**Table 10**
Normalizations of the Diffuse Components, Integrated Flux, and Likelihoods for the Arc Fits with M31 Components

| Component | Arc Full (PL) | Arc North and South | Flux ($\times 10^{-9}$) (ph cm$^{-2}$ s$^{-1}$) | Intensity ($\times 10^{-8}$) (ph cm$^{-2}$ s$^{-1}$ sr$^{-1}$) |
|---|---|---|---|---|
| H I $\pi^0$, A5 | $0.85 \pm 0.05$ | $0.88 \pm 0.05$ | $159.8 \pm 9.1$ | $67.9 \pm 3.9$ |
| H I $\pi^0$, A6 | $0.9 \pm 0.2$ | $1.0 \pm 0.2$ | $10.3 \pm 2.5$ | $4.4 \pm 1.1$ |
| H I $\pi^0$, A7 | $2.8 \pm 0.4$ | $2.9 \pm 0.4$ | $15.3 \pm 2.1$ | $6.5 \pm 0.9$ |
| $H_2$ $\pi^0$, A5 | $2.7 \pm 0.3$ | $2.7 \pm 0.3$ | $3.7 \pm 0.4$ | $1.6 \pm 0.2$ |
| IC, A5 | $2.2 \pm 0.2$ | $2.2 \pm 0.2$ | $115.2 \pm 8.6$ | $49.0 \pm 3.7$ |
| IC, A6 – A7 | $1.2 \pm 0.4$ | $1.0 \pm 0.4$ | $20.1 \pm 7.0$ | $8.6 \pm 3.0$ |
| IC, A8 | $88.5 \pm 19.0$ | $59.7 \pm 20.2$ | $11.0 \pm 3.6$ | $4.7 \pm 1.5$ |
| $-\log L$ | 142933 | 142919 | ... | ... |

**Note**. — Columns 2 and 3 give the best fit normalizations for the diffuse components. The last two columns report the total integrated flux and intensity between 1–100 GeV for the arc north and south fit. The bottom row gives the resulting likelihood for each respective fit. Intensities are calculated by using the total area of FM31, which is 0.2352 sr.

**M31-related geometry:**

IG : $0° < r \leq 0.4°$ (5.5 kpc)

SH : $0.4° < r \leq 8.5°$ (117 kpc)

FOH : $r > 8.5°$ ( $\sim$ 200 kpc)

- Uniform intensity templates centered at M31.
- See slide 16 for an image of template boundaries.
- See extra slides for further analysis of symmetry.

**Table 12**
Results for the Arc Template (North and South, PLEXP) and M31 Components

| Template | area (sr) | TS | Flux ($\times 10^{-9}$) (ph cm$^{-2}$ s$^{-1}$) | Energy Flux ($\times 10^{-12}$) (erg cm$^{-2}$ s$^{-1}$) | Intensity ($\times 10^{-8}$) (ph cm$^{-2}$ s$^{-1}$ sr$^{-1}$) | Counts | Index $\alpha$ | Cutoff, $E_c$ (GeV) |
|---|---|---|---|---|---|---|---|---|
| Arc North | 0.033864 | 438 | $15.5 \pm 1.3$ | $78.9 \pm 6.4$ | $45.8 \pm 3.8$ | 4027 | $2.2 \pm 0.1$ | $84.5 \pm 100.4$ |
| Arc South | 0.046368 | 395 | $11.8 \pm 0.7$ | $47.8 \pm 4.1$ | $25.4 \pm 1.5$ | 3155 | $2.5 \pm 0.1$ | $100.0 \pm 6.6$ |
| FM31 Inner Galaxy | 0.000144 | 53 | $0.5 \pm 0.08$ | $1.7 \pm 0.4$ | $347.2 \pm 55.6$ | 139 | $2.8 \pm 0.3$ | $100.0 \pm 10.6$ |
| FM31 Spherical Halo | 0.0684 | 39 | $4.5 \pm 1.2$ | $22.0 \pm 6.4$ | $6.6 \pm 1.8$ | 1223 | $0.9 \pm 0.8$ | $4.0 \pm 3.6$ |
| FM31 Far Outer Halo | 0.166656 | 30 | $3.8 \pm 1.3$ | $31.6 \pm 8.7$ | $2.3 \pm 0.8$ | 1020 | $-1.8 \pm 1.3$ | $1.8 \pm 0.6$ |

**Note**. — The TS is defined as $-2\Delta \log L$, and it is the value reported by pylikelihood, without refitting. Fits are made with a model with exponential cut off $dN/dE \propto E^{-\alpha} \exp(-E/E_c)$.

- **Three spherically symmetric templates centered at M31 are added to the model: inner galaxy (IG), spherical halo (SH), and far outer halo (FOH)**.
- Templates are given PLEXP spectral models and fit simultaneously with other components of the IEM, including the arc template. Two fit variations are performed, amounting to two different variations in the arc template: full arc with PL, arc north and south with PLEXP.
- Also tried different spectral models for M31-related templates: results are qualitatively consistent with PLEXP spectra.
- IG, SH, and FOH are detected at the significance levels (sigma) of 7, 7, and 5, respectively. These are the TS values reported by pylikelihood without refitting. Results for the two fit variations are similar.
- Defining the null model as all components except for the SH and FOH, **the alternative model which includes the halo templates is preferred at the confidence level of 8 sigma**. This is a more conservative estimate of the significance of the outer halo templates.
- **The M31-related components are able to flatten the positive residual emission between ~3-20 GeV, and are physically motivated**.
- Results for the IG are consistent with previous studies. **Spectra for the SH and FOH are significantly different than all other diffuse components in FM31**.
- **Diffuse components all in reasonable agreement with GALPROP predictions**.

# Interpretation: M31-Related Components

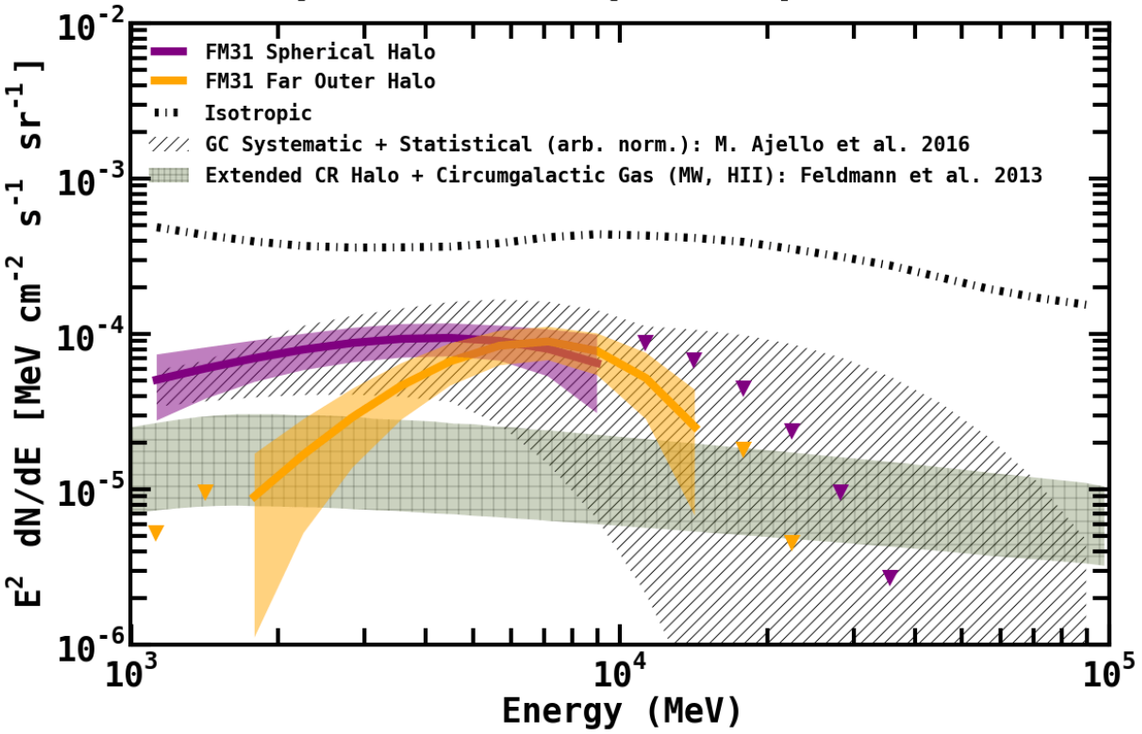


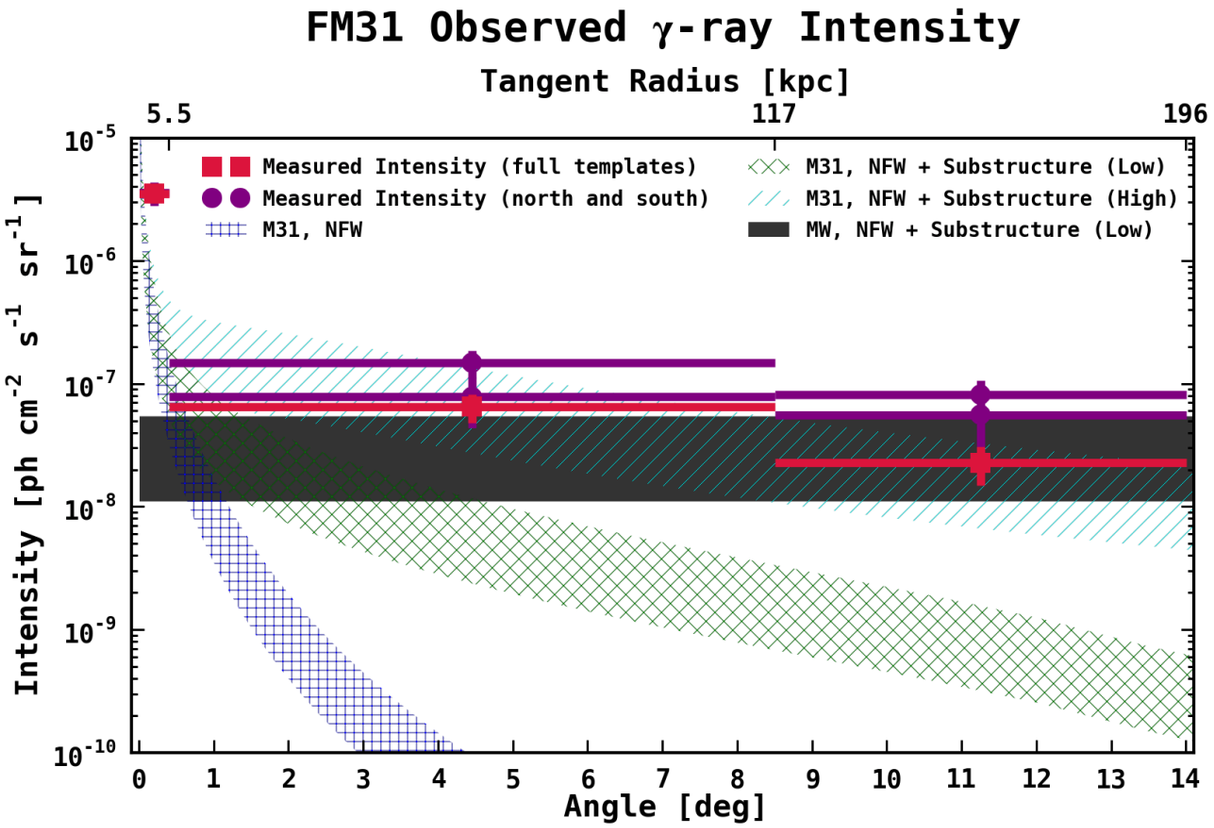


- Properties of M31's DM halo remain highly uncertain, i.e. geometry, extent, and substructure content. Likewise for the MW's DM halo.
- **We compare the observed excess with (simplified) predictions for a DM signal that originates from the M31 halo, with a spectrum and annihilation cross-section consistent with a DM interpretation of the GC excess**.
- We consider the contribution from both the M31 halo and the MW halo along the line of sight, since the MW component has not been explicitly accounted for in our analysis, and may be at least partially embedded within the isotropic component and other IEM components.
- We consider different assumptions for the amount of DM substructure in M31 (and the MW), and **we find that if a cold DM scenario is assumed that includes a large boost factor due to substructures, the observed excess emission is consistent with this interpretation**.
- Granted, however, the exact partitioning of individual contributions to the signal remains unclear, i.e. primary emission from M31's DM halo, secondary emission in M31, emission from the local DM filament between M31 and the MW, and emission from the MW's DM halo along the line of sight.

# The Structured Emission in FM31

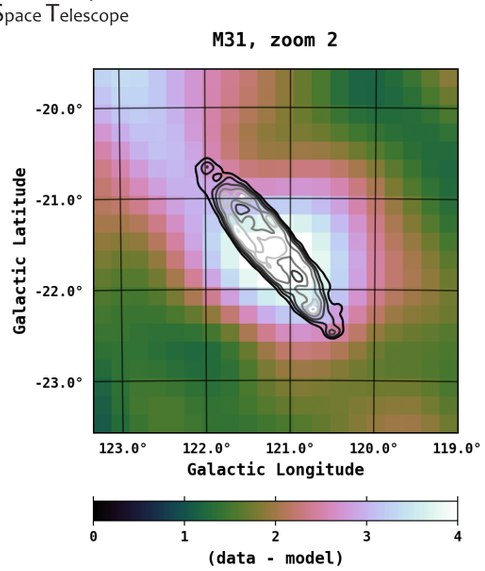


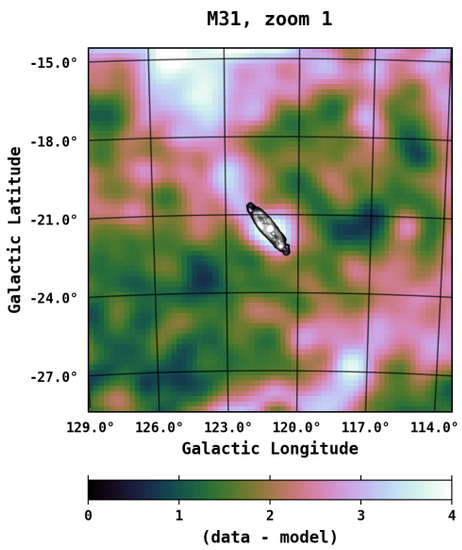


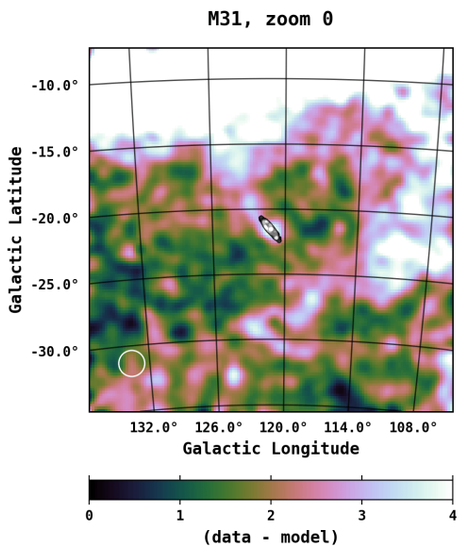


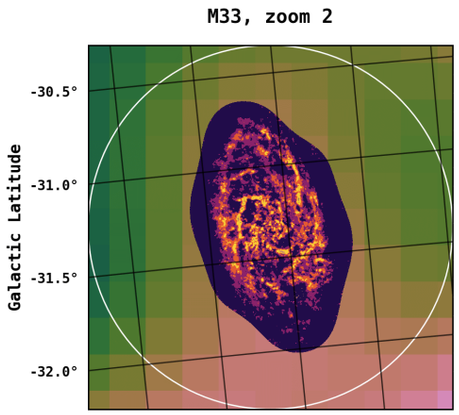


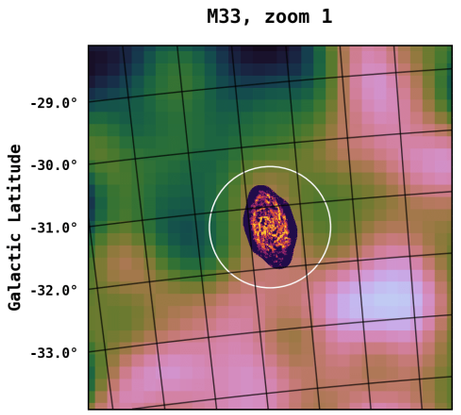


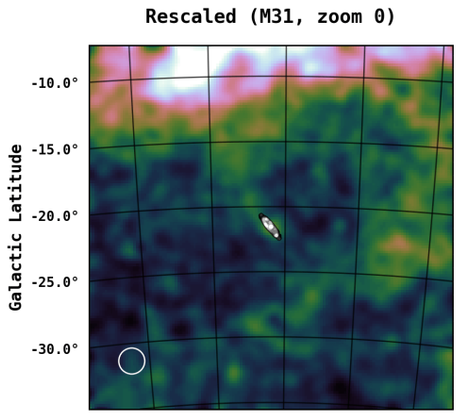


- The characterization of the gas-related emission in FM31 is a significant systematic uncertainty.
- To gauge the full extent of this uncertainty we observe the structured emission in FM31 in a (semi) model-independent way by removing the H I-related templates from the model. We also remove the two point sources closest to the M31 disk, and the new sources.
- This feature in the emission is found to be positionally coincident with the M31 cloud, which is a highly extend H I cloud centered in projection on M31, possibly associated with the M31 system. Further investigation is left for a follow-up study.
- The arc feature is also clearly visible in the emission.

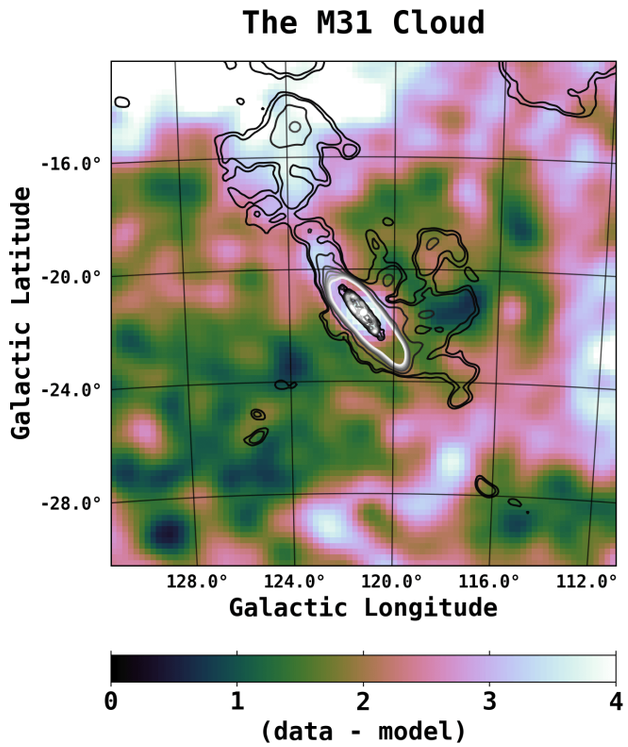


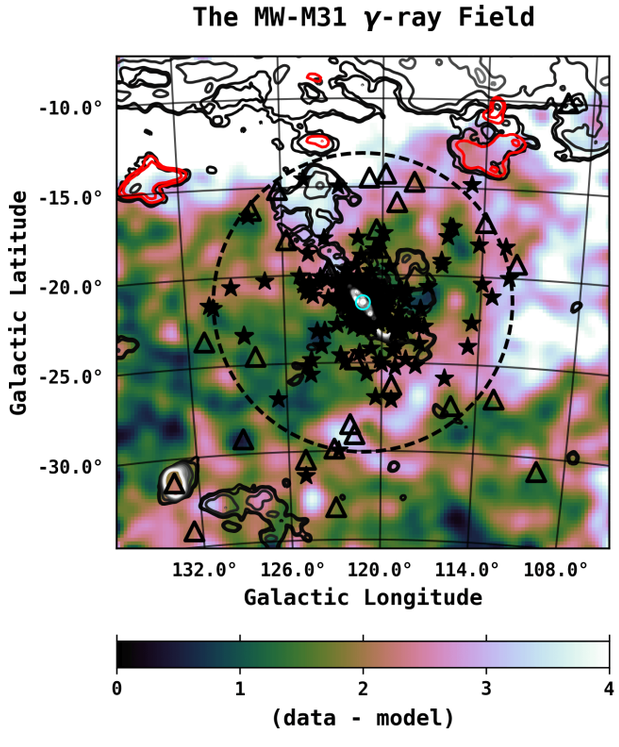

# Acknowledgements

I would like to thank my advisor, Simona Murgia; my committee, Mike Cooper and Manoj Kaplinghat; all my collaborators, including many members of the *Fermi*-LAT Collaboration, my friends and fellow classmates, and more generally the faculty and staff in the Department of Physics and Astronomy at UCI.